Towards

Realistic models of mantle convection

(651-4008-00 G)

Schedule

- In an effort to understand the dynamics and origins of terrestrial tectonics, we embark on a tour of different convective systems
- We will example mantle convection systems:
  - as a function of Rayleigh number
  - with bottom heated boundary conditions
  - which are internally heated
  - with temperature dependent viscosity
  - with non-Newtonian viscosity
  - with plastic yielding
  - phase transitions
  - containing compositional variations
  - with a free surface boundary condition
  - in three-dimensional geometry

Thermal convection

http://dreamtigers.wordpress.com/2011/05/11/plate-tectonic-metaphor-illustrations-cmu/

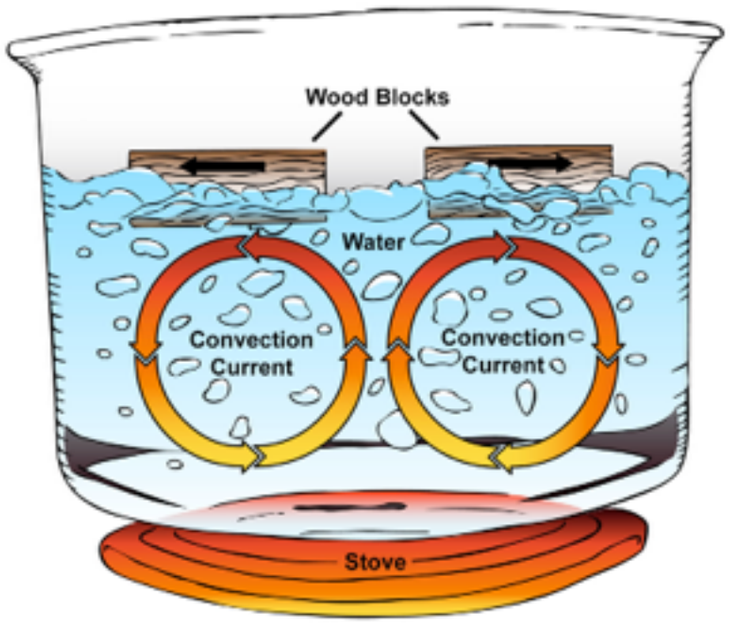

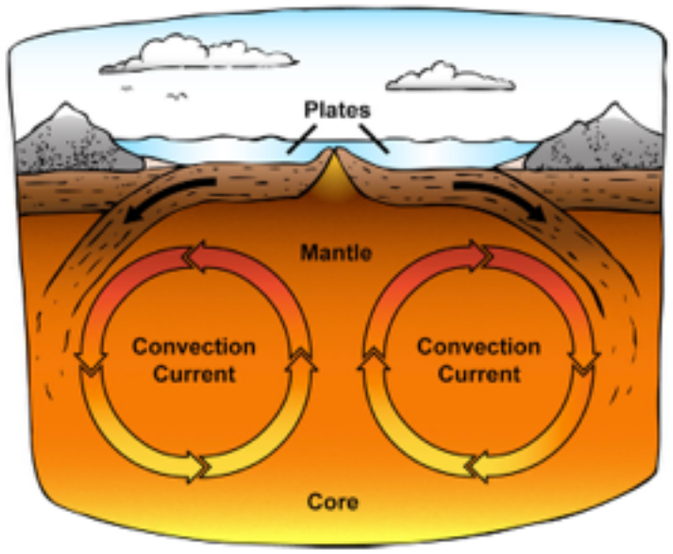

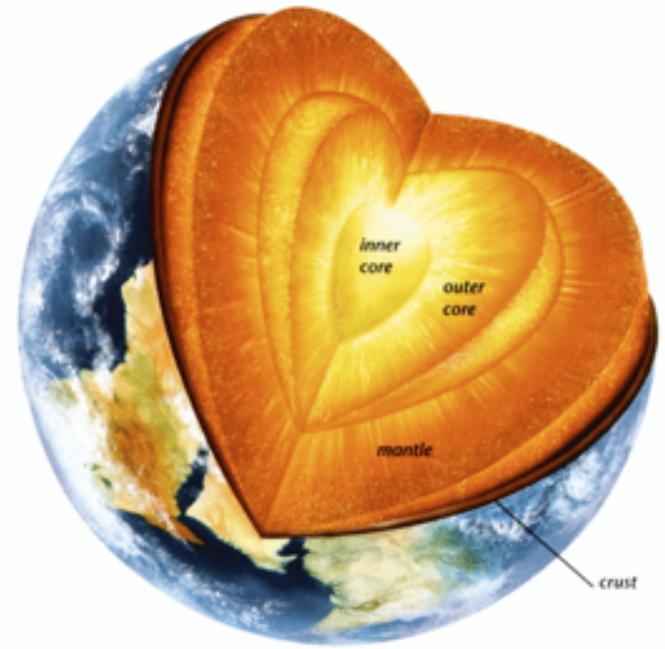

Variations in temperature cause small changes in the fluid density

Buoyancy forces cause cold (compressed, i.e. higher density) material to sink

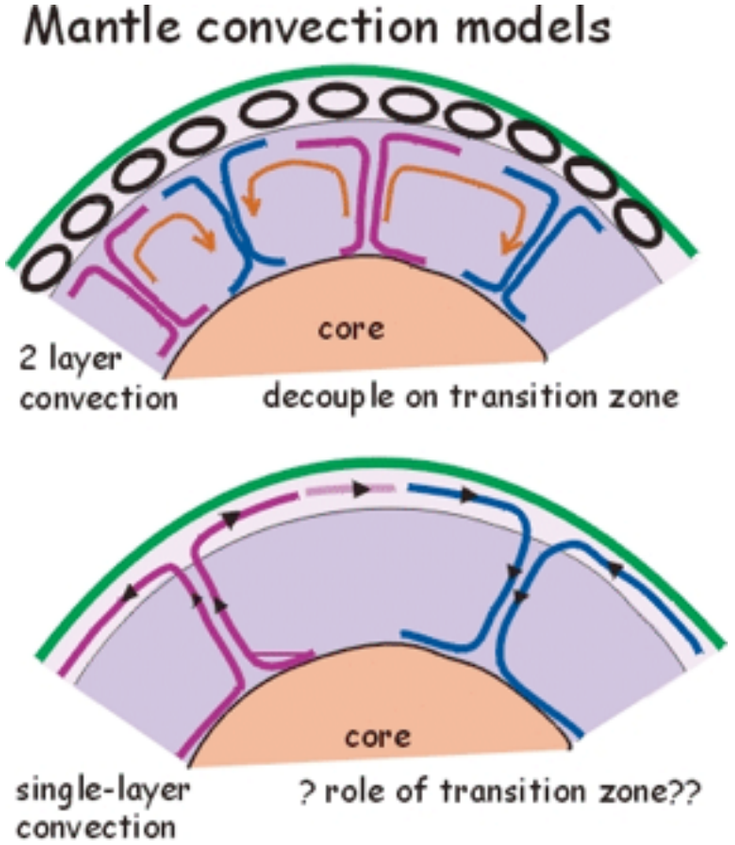

http://www.see.leeds.ac.uk/structure/dynamicearth/convection/models.htm

http://asapscience.tumblr.com/post/50419005208/the-earths-center-is-out-of-sync-we-all-know

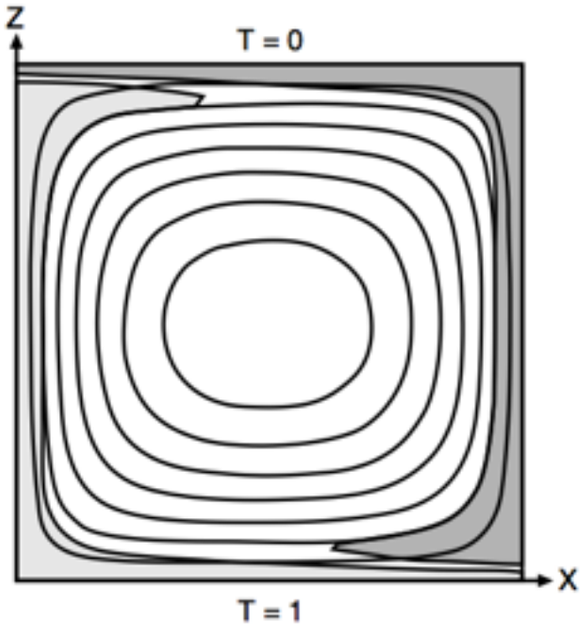

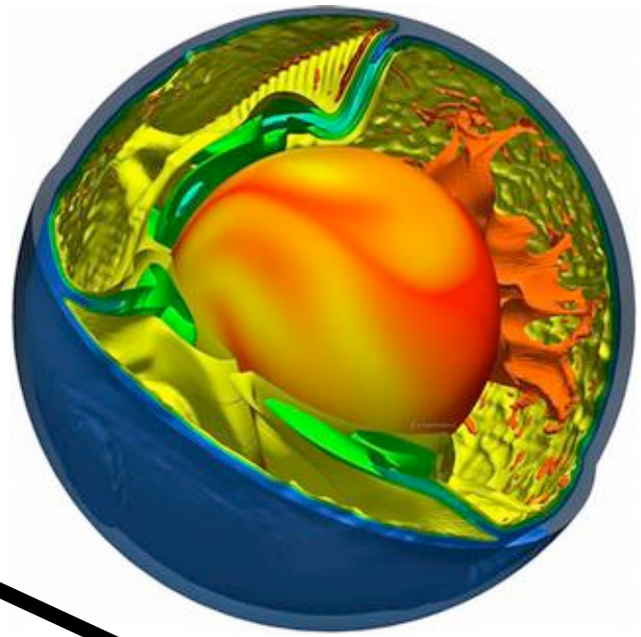

how to go from here … to here

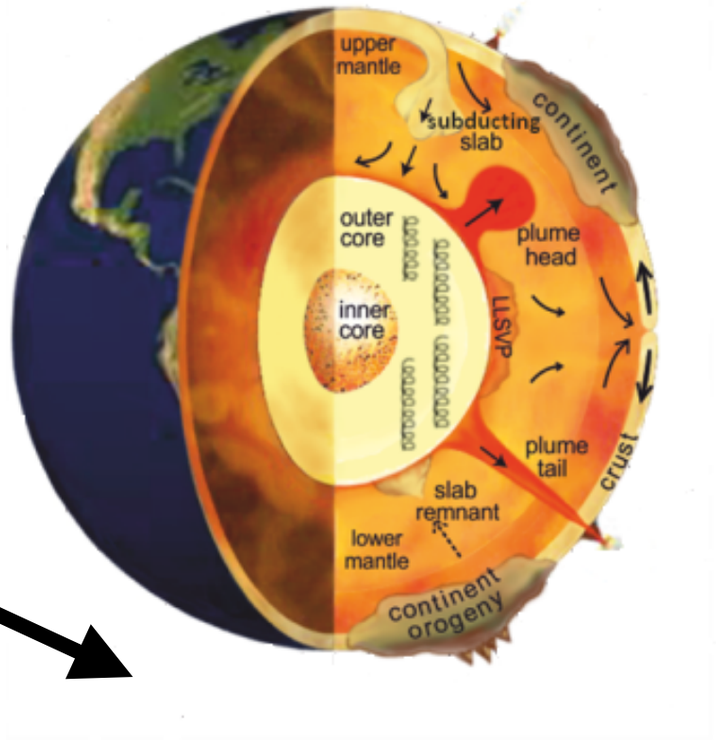

Fluid constitutive law

- Viscous

$$\tau_{ij} = 2\eta\,\tilde{\epsilon}_{ij}$$

deviatoric stress ← τ_{ij}

$\tilde{\epsilon}_{ij}$ → ***deviatoric strain rate [1/s]***

η → ***viscosity [Pa s]***

- Incompressible

$$\tau_{ij} = 2\eta\,\epsilon_{ij} \longrightarrow \textbf{\textit{strain rate}}$$

- Expanded form (2D)

$$\tau_{xx} = 2\eta\,\epsilon_{xx} = 2\eta\,\frac{\partial v_x}{\partial x}$$

$$\tau_{zz} = 2\eta\,\epsilon_{zz} = 2\eta\,\frac{\partial v_z}{\partial z}$$

$$\tau_{xz} = 2\eta\,\epsilon_{xz} = \eta\left(\frac{\partial v_x}{\partial z} + \frac{\partial v_z}{\partial x}\right)$$

Boussinesq

- Thermal variations in a fluid lead to small amounts of expansion / contraction.
- Expansion results in lowering of density, e.g. resulting in a buoyancy force —> leading to thermal convection

$$\rho = \rho_0 + \rho' \xrightarrow{\text{perturbation}} \rho' \ll \rho_0$$

ρ_0: Reference density

$$\rho' = -\rho_0 \alpha_v \left(T - T_0\right)$$

T_0: Reference temperature corresponding to ref. density

α_v: coefficient of thermal expansivity [1/K]

Non-dimensionalisation

(1) Dimensional form:

$$-\nabla p + \eta \nabla^2 \boldsymbol{v} = \rho_0 \left(1 - \alpha(T - T_0)\right) g \hat{\mathbf{e}}_z$$

$$\nabla \cdot \boldsymbol{v} = 0$$

$$\frac{DT}{Dt} = \kappa \nabla^2 T$$

(2) Perturbation from background state:

$$-\nabla p + \eta \nabla^2 \boldsymbol{v} = -\rho_0 \alpha T g \hat{\boldsymbol{e}}_z$$

$$\nabla \cdot \boldsymbol{v} = 0$$

$$\frac{DT}{Dt} = \kappa \nabla^2 T$$

(3) Scaling:

$$\boldsymbol{x}' = \boldsymbol{x}/h$$

$$t' = t/(h^2/\kappa)$$

$$T' = T/\Delta T$$

$$\boldsymbol{v}' = \boldsymbol{v}/(\kappa/h)$$

$$p' = p/(\eta\kappa/h^2)$$

(4) Non-dimensional form:

$$-\nabla' p' + \nabla'^2 \boldsymbol{v}' = -Ra T' \hat{\boldsymbol{e}}_z$$

$$\nabla' \cdot \boldsymbol{v}' = 0$$

$$\frac{DT'}{Dt'} = \nabla'^2 T'$$

$$\longrightarrow \quad Ra = \frac{\alpha \rho_0 g \Delta T h^3}{\eta \kappa}$$

Rayleigh number

Non-dimensional numbers

Reynolds number

- inertia forces / viscous forces
- zero for the Earth on long time scales

$$Re = \frac{\rho h U}{\eta}$$

Rayleigh number

- advection / conduction
- indicates something about the vigor of convection

$$Ra = \frac{\alpha \rho_0 g \Delta T h^3}{\eta \kappa}$$

Nusslet number

- convective heat transfer / conductive heat transfer
- non-dim heat flux
- provides a measure of efficiency of heat transfer through the surface

Numerical experiments

40 years of mantle convection

1975 “Cray-1”

2014 Cray “XC30”

[Pt 1] Iso-viscous, bottom heated

$$-\nabla' p' + \nabla'^2 \boldsymbol{v}' = -RaT'\hat{\boldsymbol{e}}_z$$

$$\nabla' \cdot \boldsymbol{v}' = 0$$

$$\frac{DT'}{Dt'} = \nabla'^2 T'$$

$$Ra = \frac{\alpha \rho_0 g \Delta T h^3}{\eta \kappa}$$

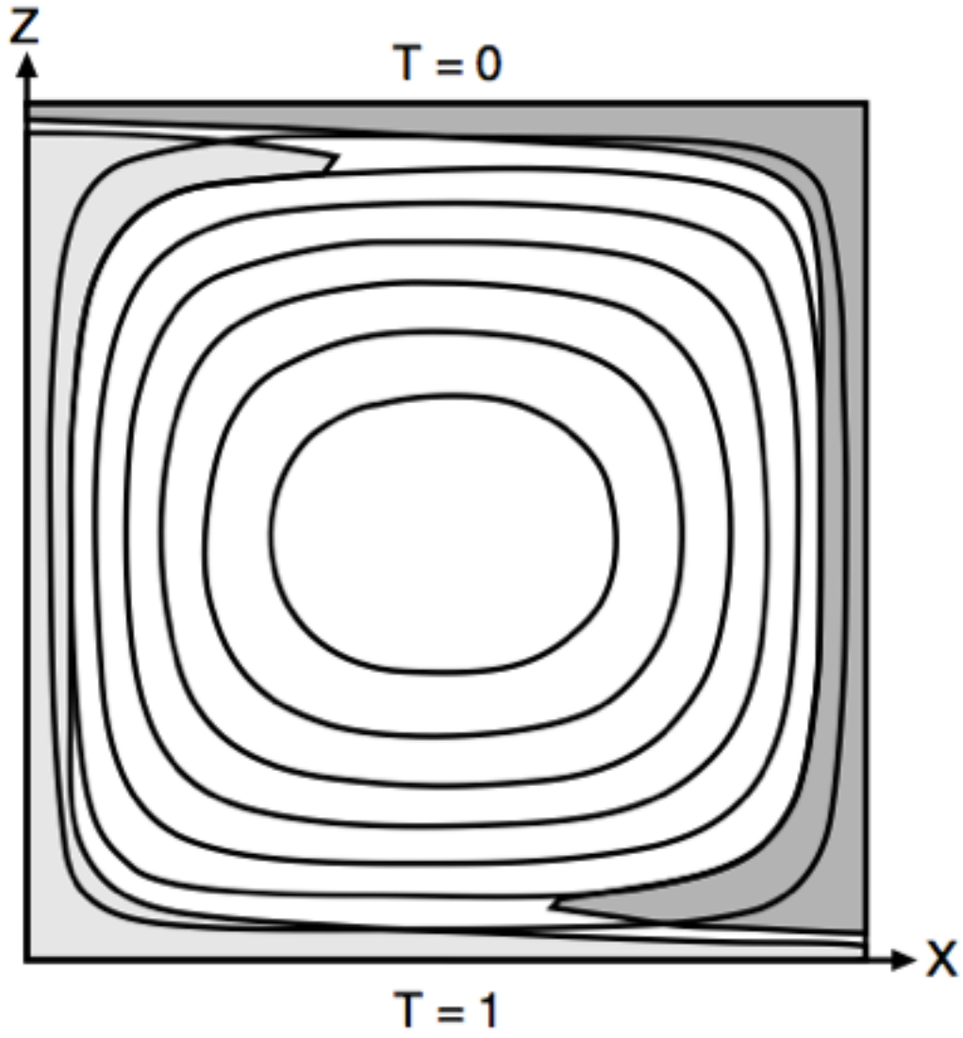

Figure 9.1. The structure of steady-state, two-dimensional, Rayleigh–Bénard convection at infinite Prandtl number, with streamlines of the motion (solid contours), hot thermal boundary layer and rising plume (light shading), and cold thermal boundary layer and sinking plume (dark shading).

Steady state

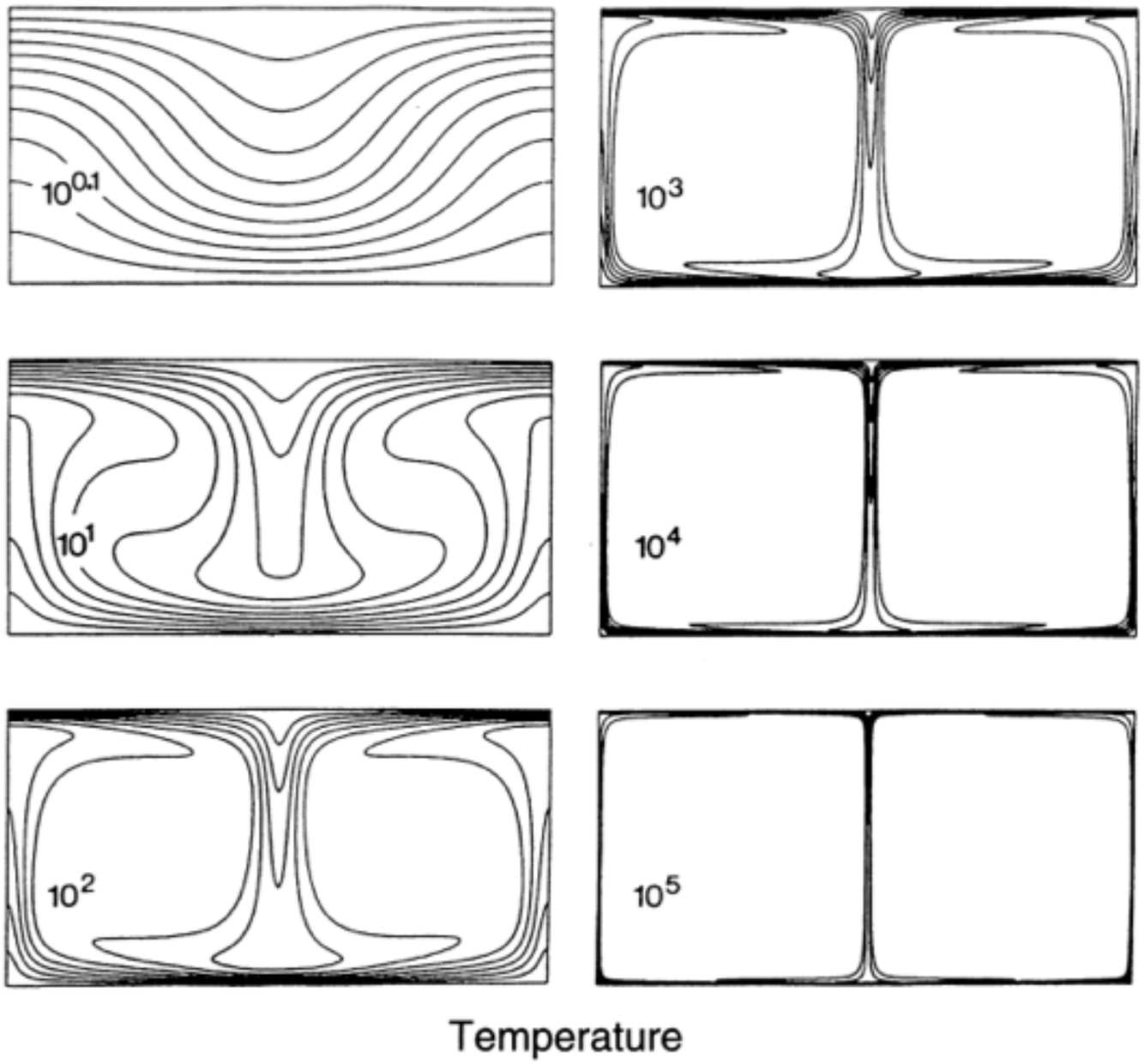

Figure 9.2. Contours of temperature for steady, two-dimensional, Rayleigh–Bénard convection in aspect ratio one cells heated from below (Jarvis, 1984), showing the development of thermal boundary layers with increasing Rayleigh number. Numbers indicate the ratio Ra/Ra_{cr}, with $Ra_{cr} = 779.27$.

Time dependence

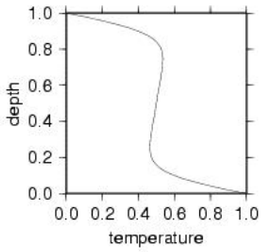

Ra=1e5

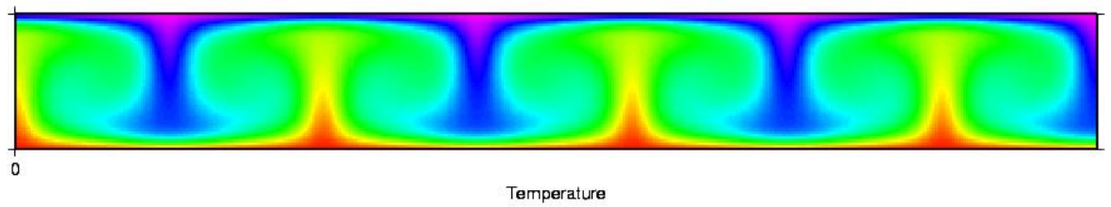

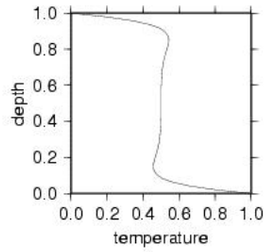

Ra=1e6

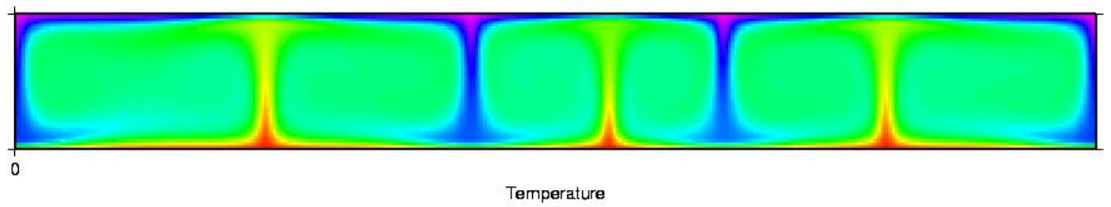

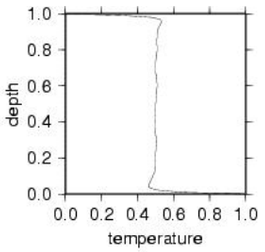

Ra=1e7

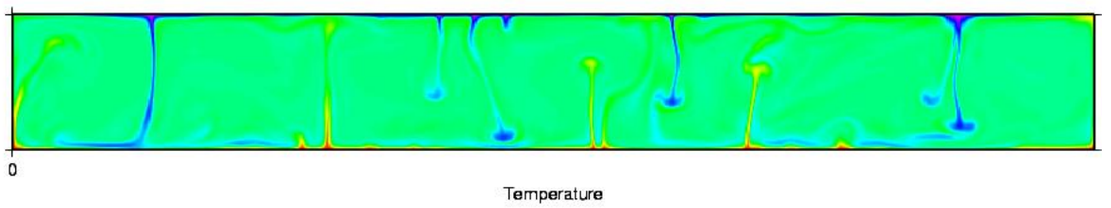

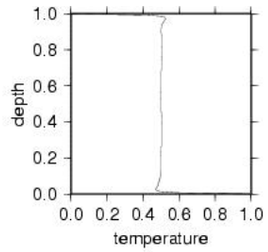

Ra=1e8

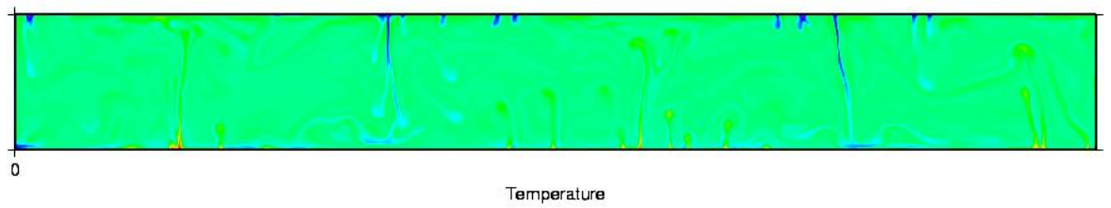

Transition to hard turbulence

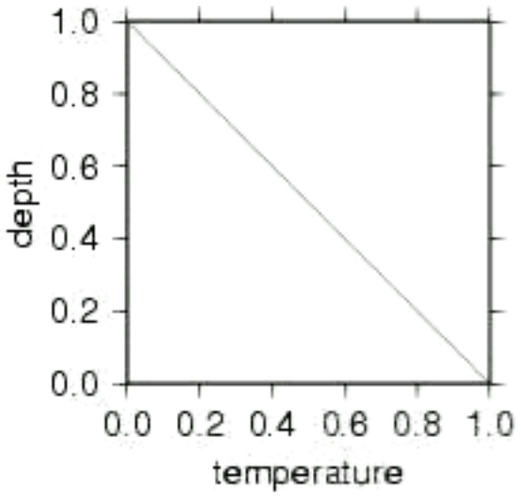

Ra = 1e6 “soft” turbulence

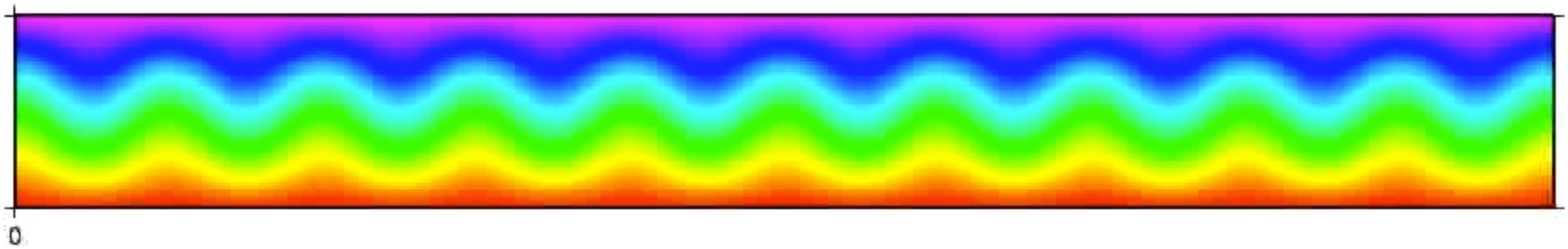

Transition to hard turbulence

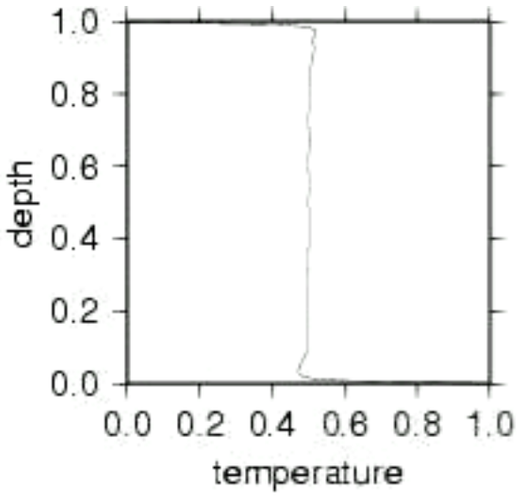

Ra = 1e8 “hard” turbulence

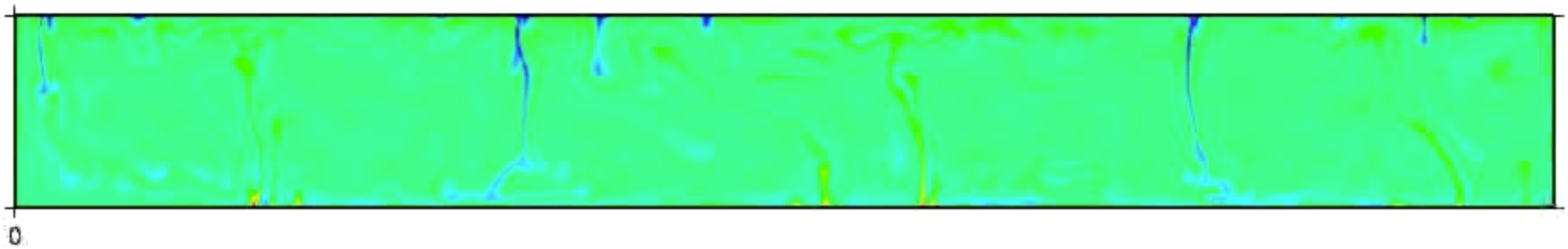

Nu-Ra scaling laws

Problem dependence

(iso-viscous: moderate Ra)

$$Nu = cRa^{\beta}$$

$$c = 0.27, \quad \beta = 0.3185$$

(iso-viscous: high Ra)

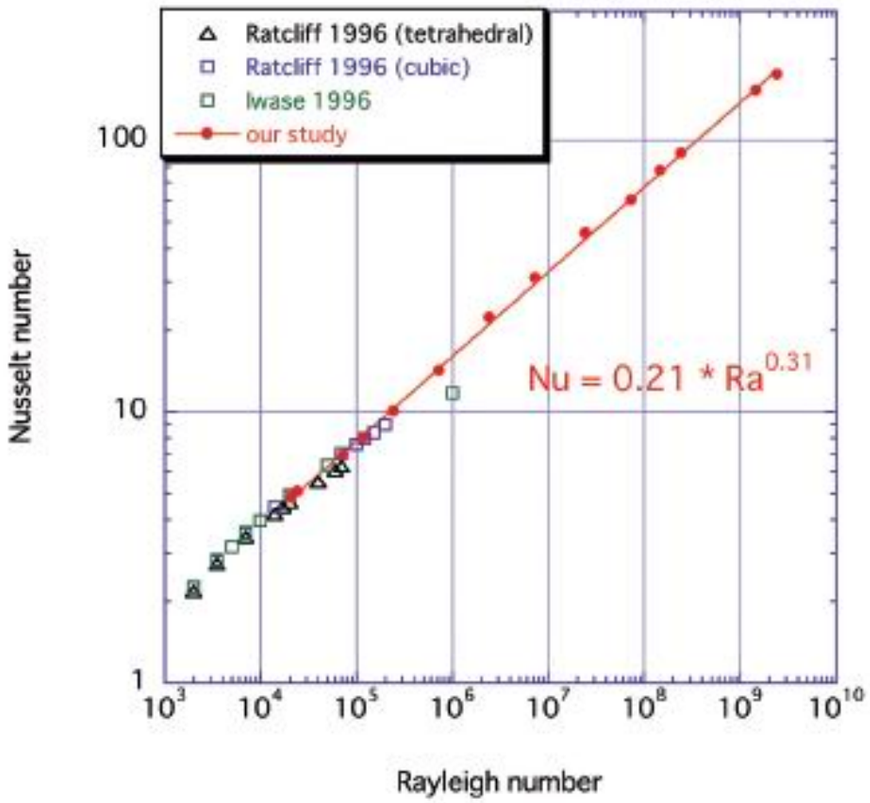

Fig. 5 Summary of the relationship between *Ra* and *Nu* for spherical shell with infinite *Pr* fluid. Our data (red points) suggests $Nu \sim Ra^{0.31}$ for wide range of *Ra*.

Fukao et al. (2008)

(variable viscosity)

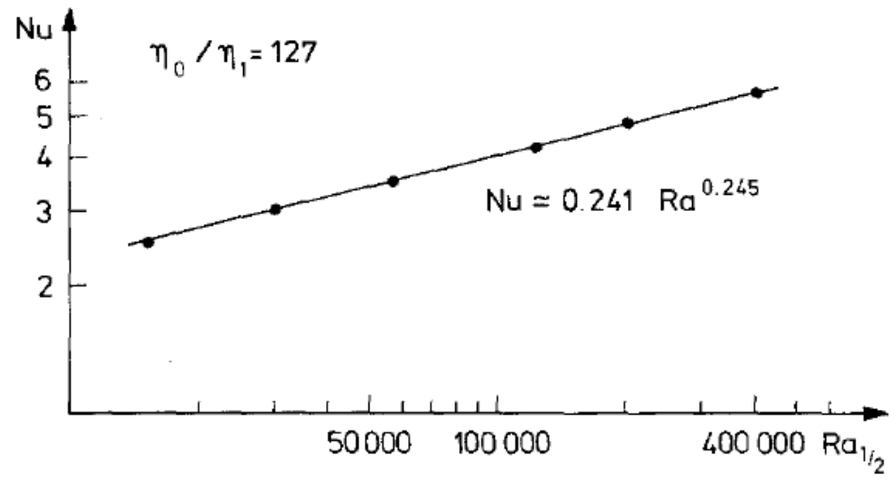

Fig. 2. Nusselt–Rayleigh number relationship for a fluid with rheological properties as used by Booker (1976) and a fixed viscosity ratio of 127. Upper and lower boundary are rigid.

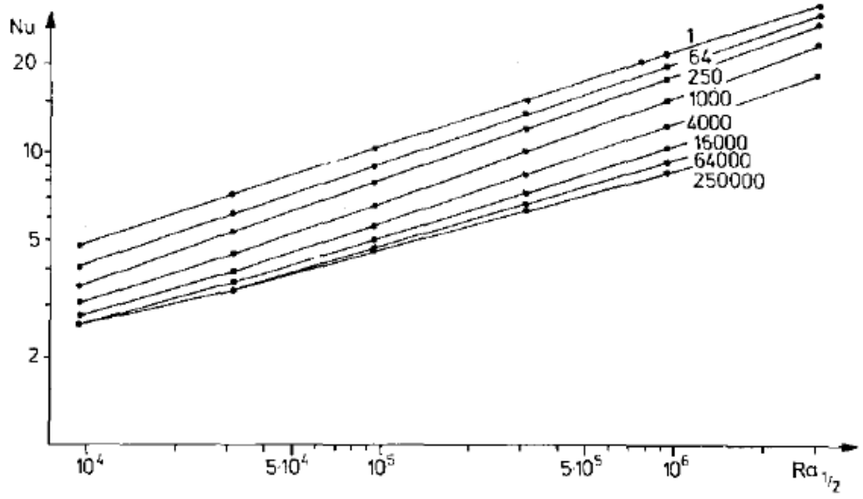

Fig. 7. Nusselt number versus Rayleigh number calculated with the viscosity at the mean of top and bottom temperature for variable viscosity convection with free boundaries. The numbers attached to the curves indicate the viscosity ratio

Christensen (1984)

[Pt 2] Iso-viscous, basal heating

- Replace constant temperature at the base with constant heat flux *q*,
- From Fourier's law

$$\Delta T = \frac{qh}{k}$$

- Define new Rayleigh number…

$$Ra_q = \frac{\alpha g \rho_0 q h^4}{k \kappa \eta}$$

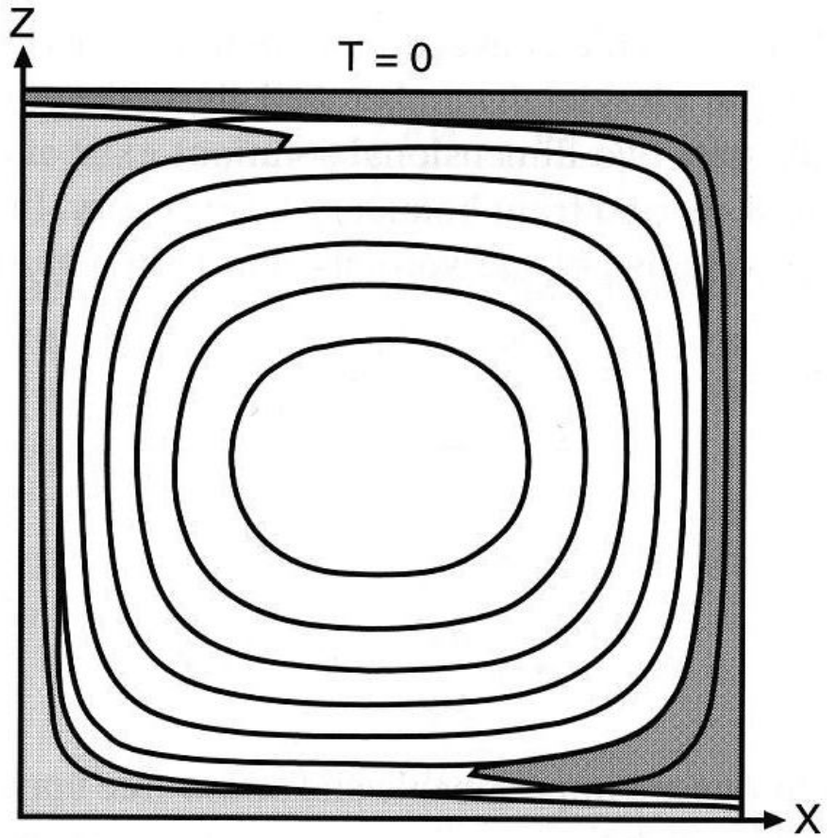

q

[Pt 3] Iso-viscous, internal heating

- Introduce an internal heat source (e.g. radiogenic).

- Conservation of energy equation becomes

$$\frac{DT}{Dt} = \kappa \nabla^2 T + \rho H$$

- Non-dimensional heat source

$$Q = \frac{h^2 \rho H}{k \Delta T}$$

- Define new Rayleigh number…

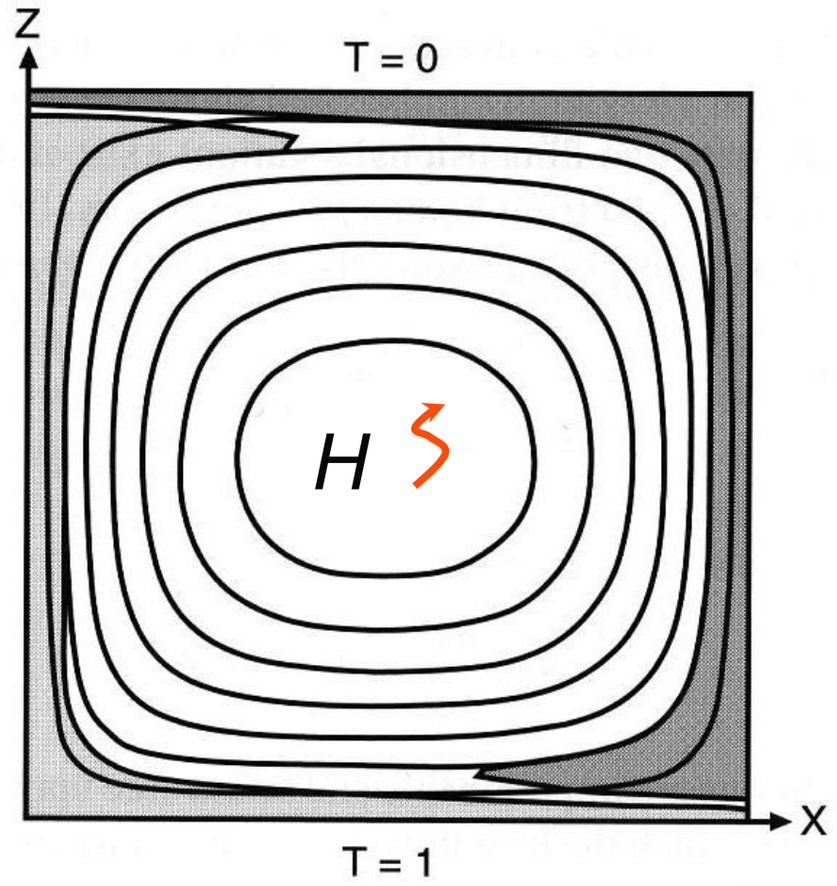

$$Ra_H = QRa = \frac{\alpha \rho_0^2 g H h^5}{k \kappa \eta}$$

Heating modes

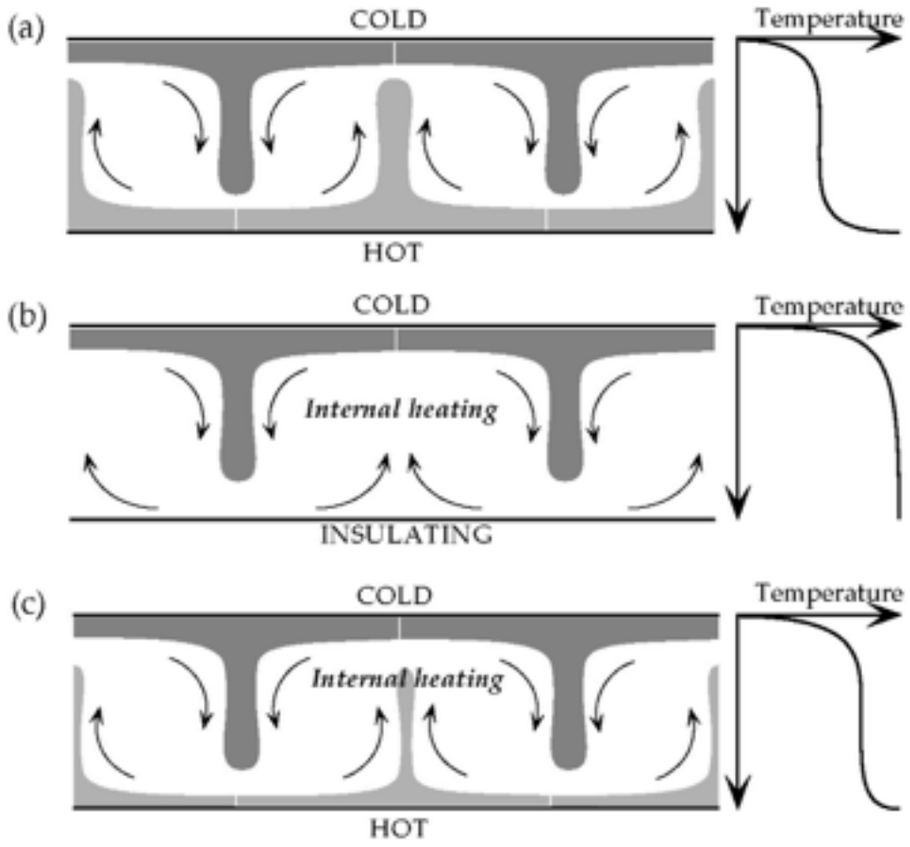

Figure 8.3. Sketches illustrating how the existence and strength of a lower thermal boundary layer depend on the way in which the fluid layer is heated.

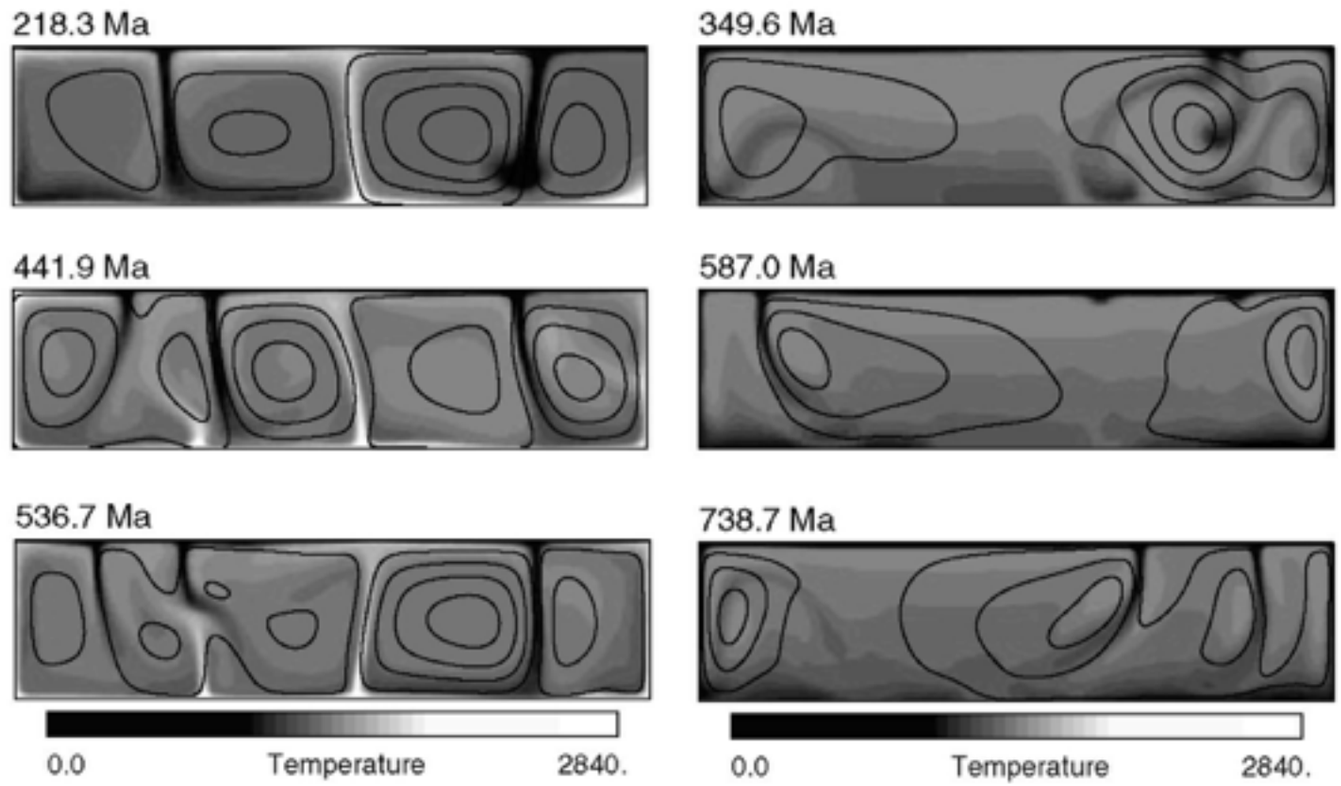

Figure 8.4. Frames from numerical models, illustrating the differences between convection in a layer heated from below (left-hand panels) and in a layer heated internally (right-hand panels). (Technical specifications of these models are given in Appendix 2.)

- Bottom / internal heating
- Passive / active upwellings
- Larger time dependence
- Bottom / upper boundary layer thickness are independent (plumes versus plates)

 (Davies, *Dynamic Earth Plates, Plumes and Mantle Convection,* 1999*)*

Internal heating: $Q = 0$

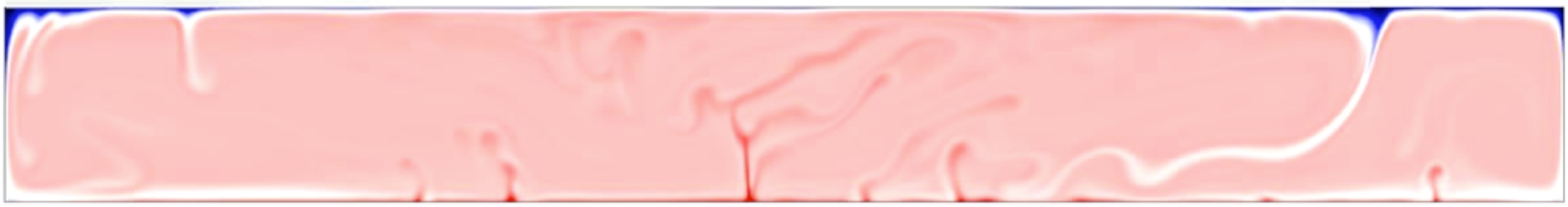

Internal heating: *Q = 20*

Internal heating: $Q = 40$

Transitions

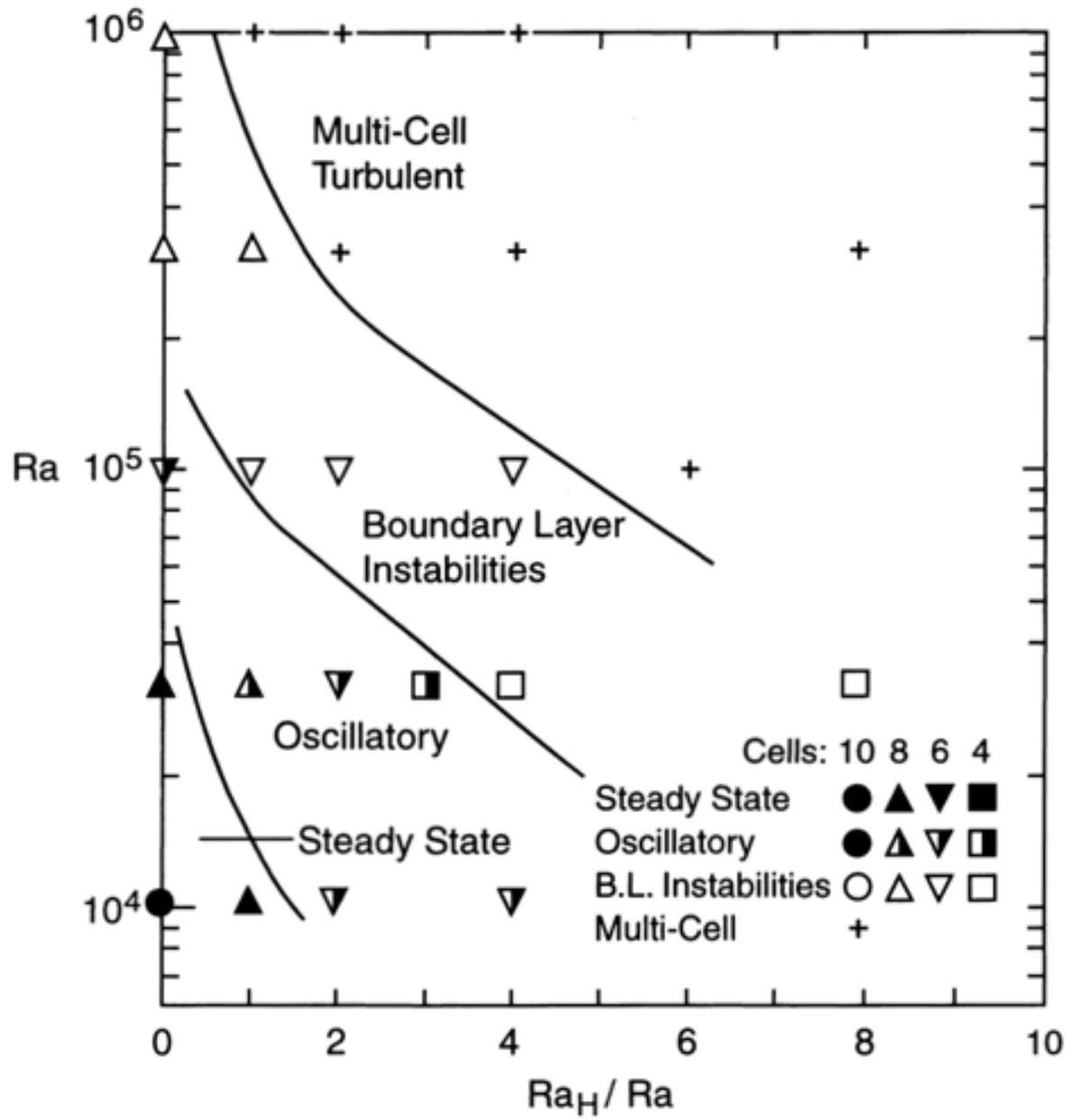

Figure 9.5. Regime diagram for two-dimensional thermal convection in an annulus with both basal and internal heating from calculations by Travis and Olson (1994). The dimensionless parameter for internal heat generation is $Q = Ra_H/Ra$.

[Pt 4] Temperature dependent viscosity

$$\eta = \eta_0 \exp\left(-\gamma T\right)$$

$$-\nabla p + \nabla \cdot \eta \left(\nabla \boldsymbol{v} + \nabla \boldsymbol{v}^T\right) = \rho_0 \left(1 - \alpha(T - T_0)\right) g \hat{\boldsymbol{e}}_z$$

- High viscosity where temperature is low (near the surface)
- Results in essentially zero velocity, strain-rate and stress in the upper regions —> “stagnant lid”
- Conductive profile in the lid
- Convection occurs under lid

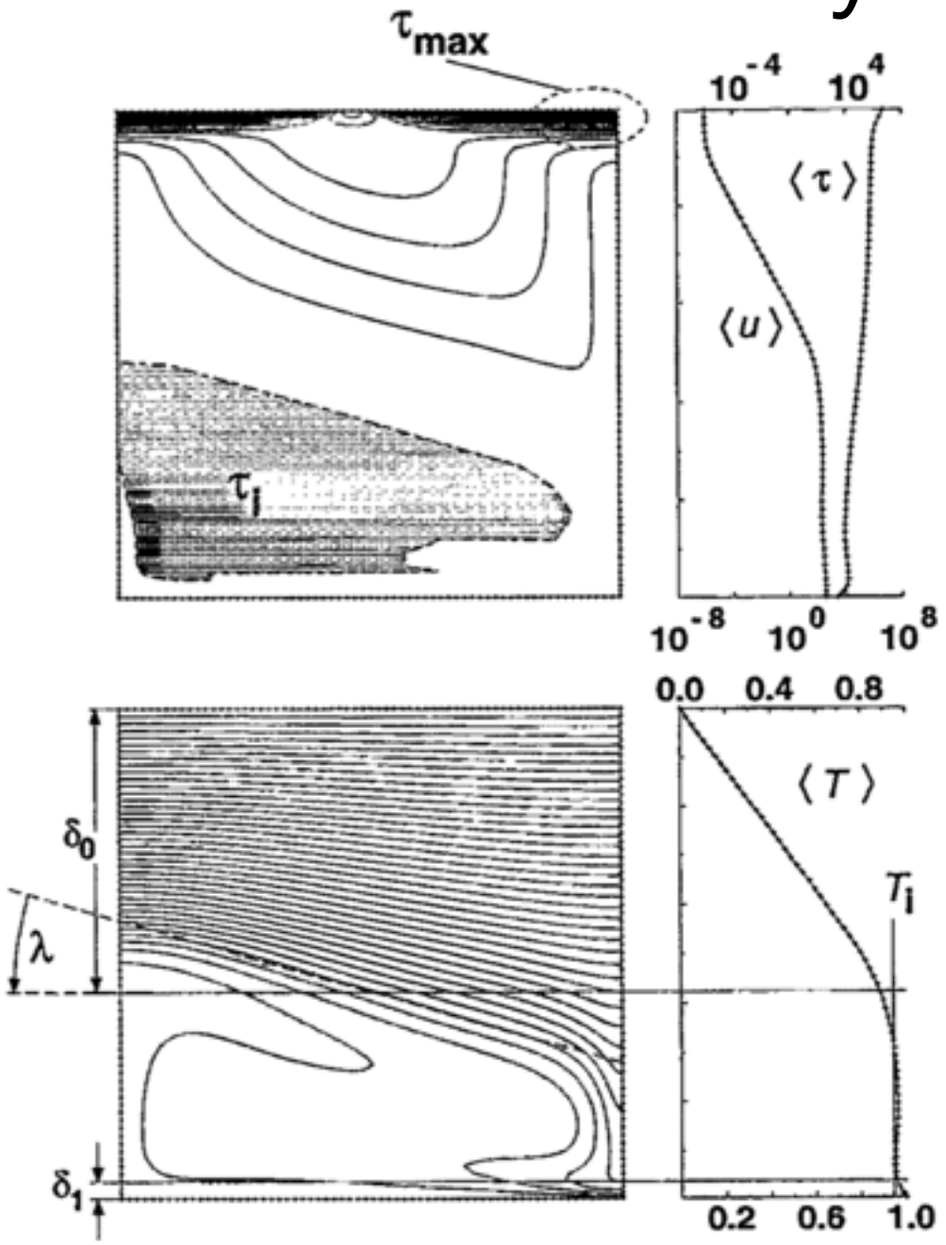

FIG. 4. Various convective parameters are shown for $Ra_1 = 10^7$, $\Delta\eta = 3 \times 10^{12}$. The stress distribution (the second invariant of deviatoric stress tensor) is shown in the top figure. The stress boundary layer[13] near the surface can clearly be seen. The maximum stress $\tau_{max} \approx 1 \times 10^7$ is located near the corner. The isothermal region over which we find the average stresses $\tau_i \approx 5 \times 10^3$ in the interiors is indicated. The horizontally averaged stresses and r.m.s. velocity are on the right. The bottom figure shows the temperature field with equally spaced isotherms and the horizontally average temperature distribution in the cell: δ_0 is the lid thickness, δ_1 is the thickness of the bottom boundary layer λ is the slope of the lid and T_i is the interior temperature.

(Moresi & Solomatov, Phys Fluids, 1995)

Stagnant lid

- Increasing viscosity ratio (from top to bottom panels)
- Lid becomes thickness as temperature dependence increases
- Heat loss through the surface becomes less efficient

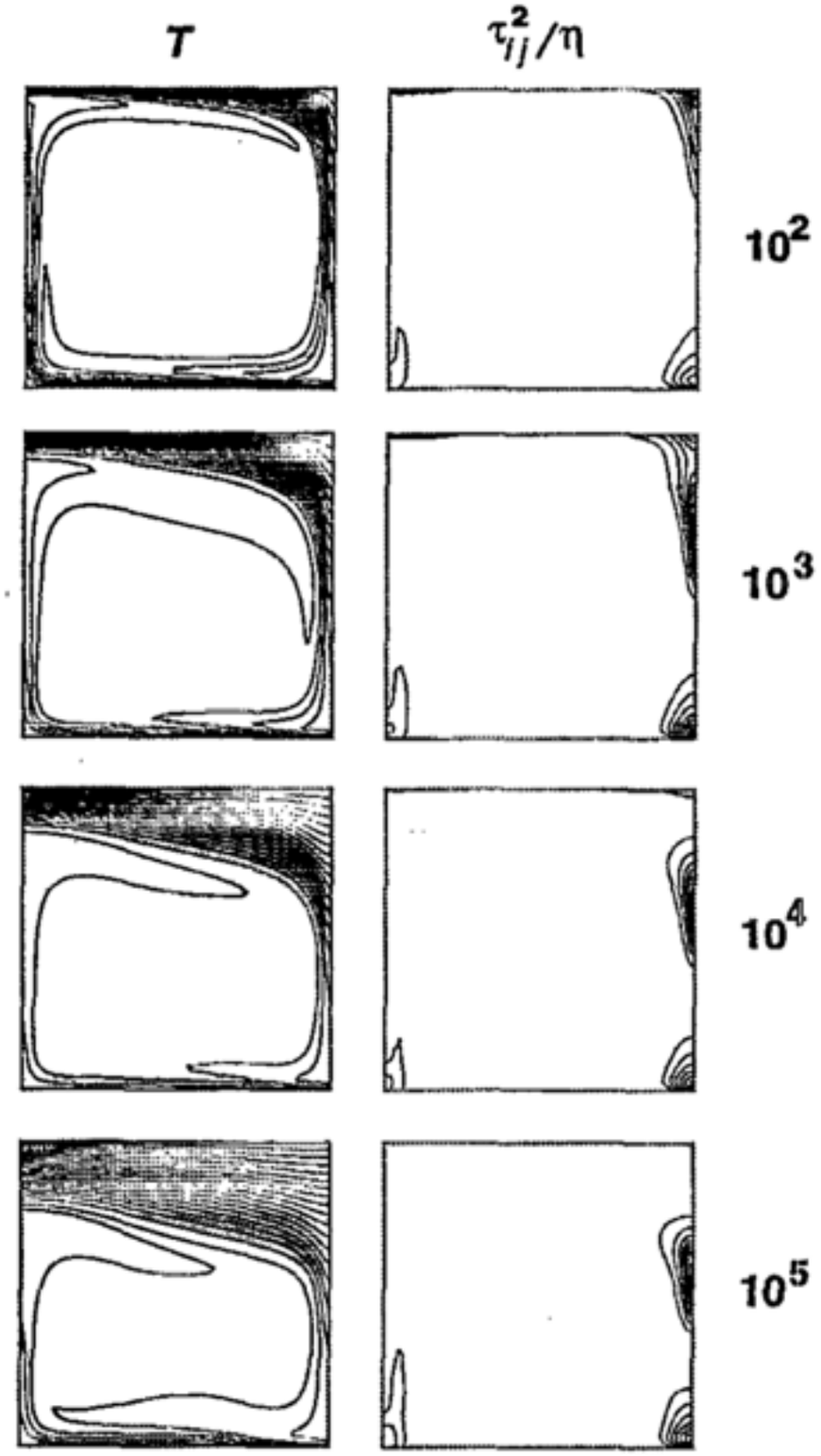

FIG. 7. The temperature T (on the left) and the viscous dissipation rate τ_{ij}^2/η are shown for $Ra_i = 10^7$ and for the viscosity contrasts $\Delta\eta = 10^2$, 10^3, 10^4, 10^5 (the number of equally spaced isotherms is the same except for the last case where two more contours are added to the hot boundary layer for a better resolution). The transition to the stagnant lid regime is seen in the change of the distribution of viscous dissipation: the region of the intense dissipation is moving away from the surface near the top right corner of the cell to the bottom of the lid where the cold plumes of the actively convecting region are formed.

(Moresi & Solomatov, Phys Fluids, 1995)

Surface motion

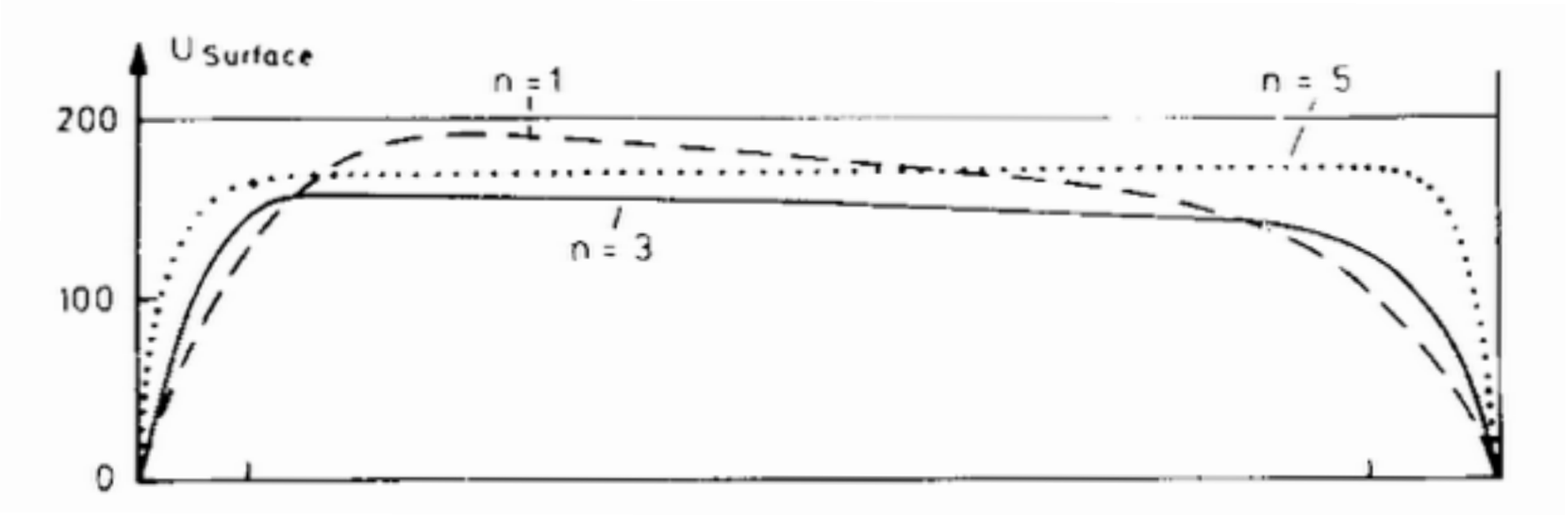

(Christensen, Geophys. J. Roy. Astron. Soc., 1984)

- Zero at cell boundaries and maximum at cell centre
- Sharp variations near cell boundaries
- Approximately constant between cell boundaries

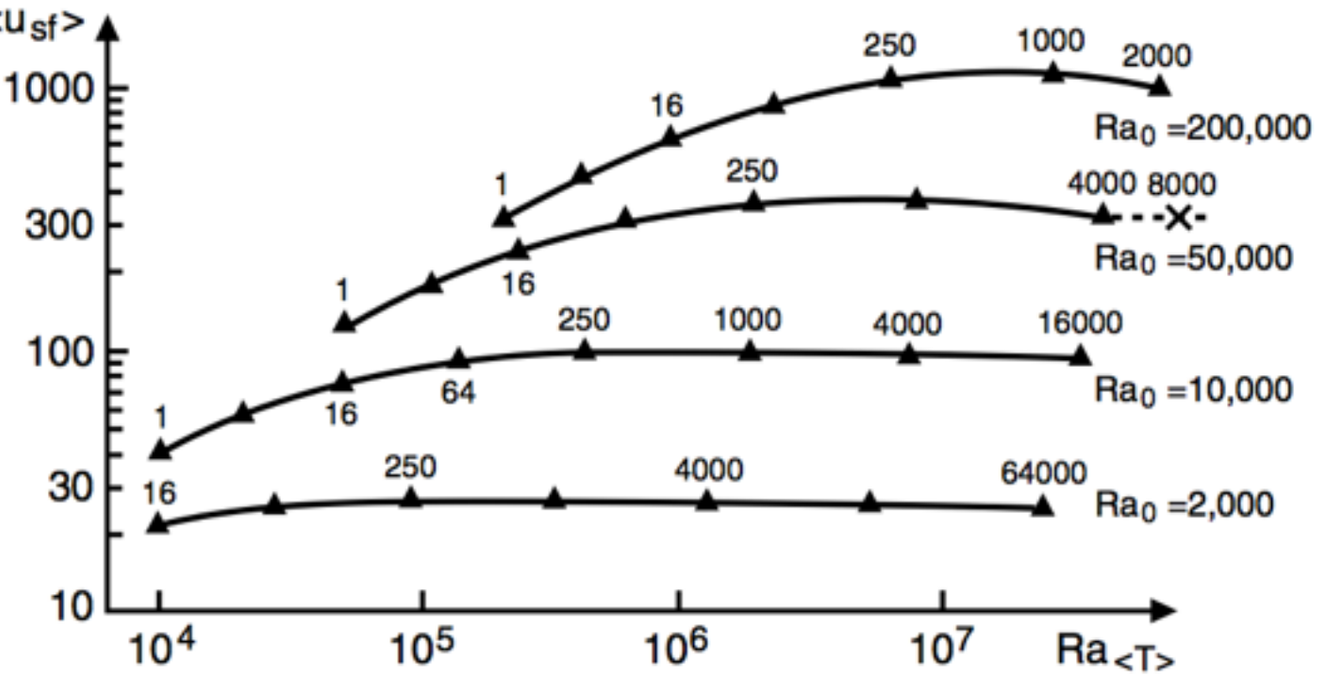

Figure 9.13. Heat transport and surface velocity in calculations of convection in a layer of fluid with temperature-dependent viscosity by Christensen (1984c). Top: Nusselt number versus Rayleigh number $Ra_{\langle T \rangle}$ based on the average mid-depth temperature. The parameter Ra_0 is based on the surface viscosity and the small numbers are the surface-to-base viscosity ratio. Bottom: Dimensionless average surface speed ($\langle u_{sf} \rangle$ or Pe) for the same calculations. The shaded region is the portion of this parameter space appropriate for the mantle.

Stagnant lid: *Visc. ratio 1e2*

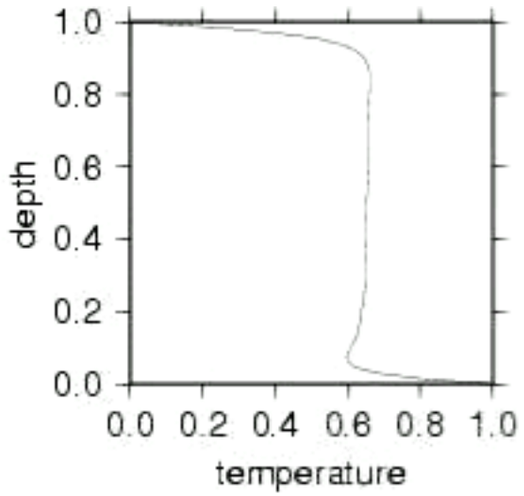

$$\frac{\eta_{\max}}{\eta_{\min}} = 10^2$$

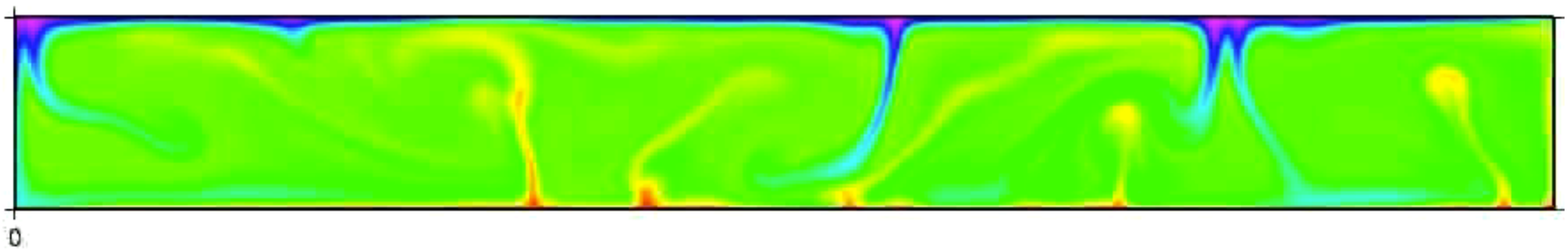

Ra = 1e6

Stagnant lid: *Visc. ratio 1e3*

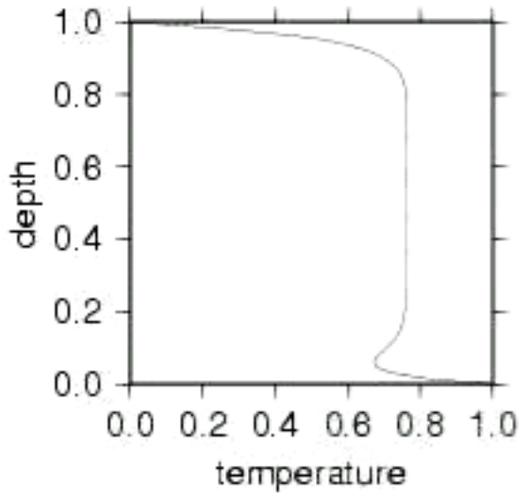

$$\frac{\eta_{\max}}{\eta_{\min}} = 10^3$$

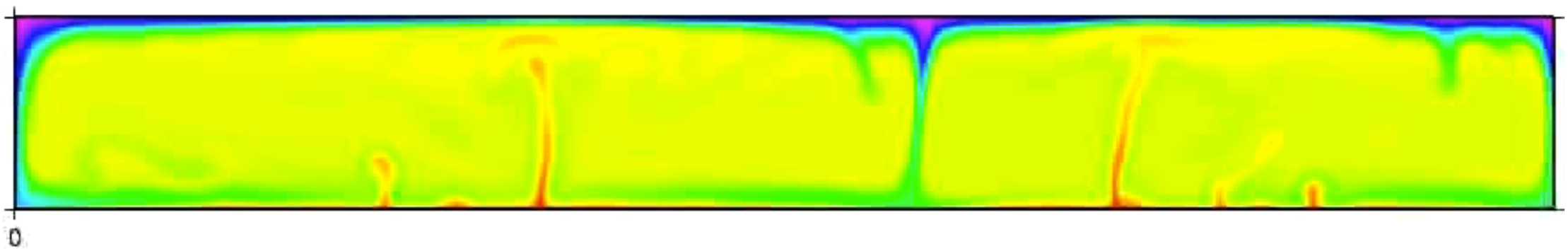

Ra = 1e6

Stagnant lid: *Visc. ratio 1e4*

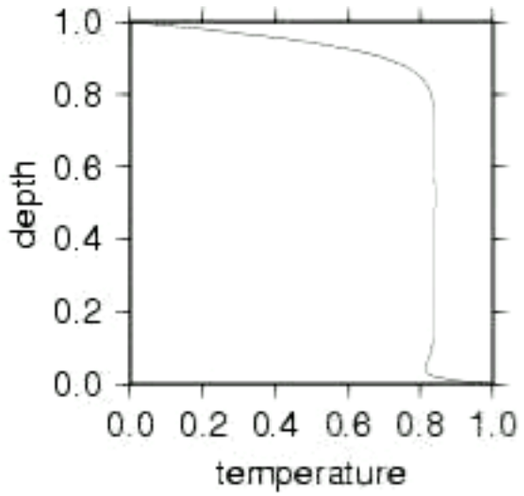

$$\frac{\eta_{\max}}{\eta_{\min}} = 10^4$$

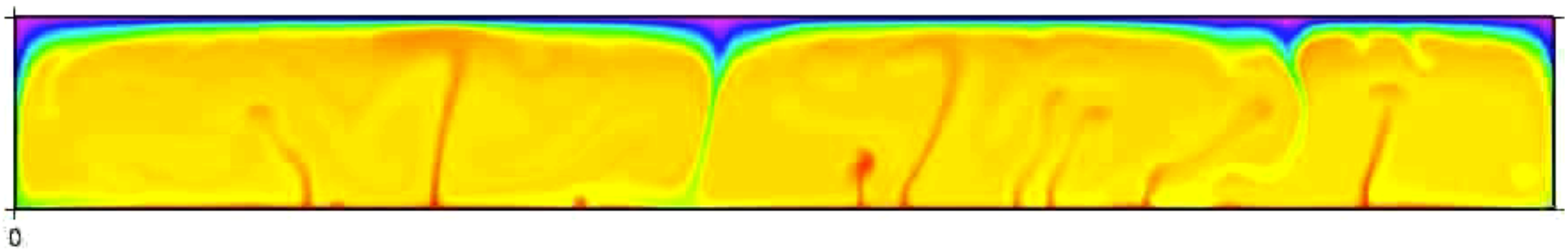

Ra = 1e6

Stagnant lid: *Visc. ratio 1e5*

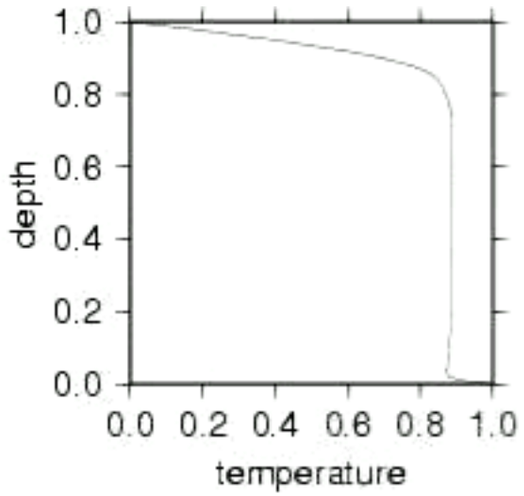

$$\frac{\eta_{\max}}{\eta_{\min}} = 10^5$$

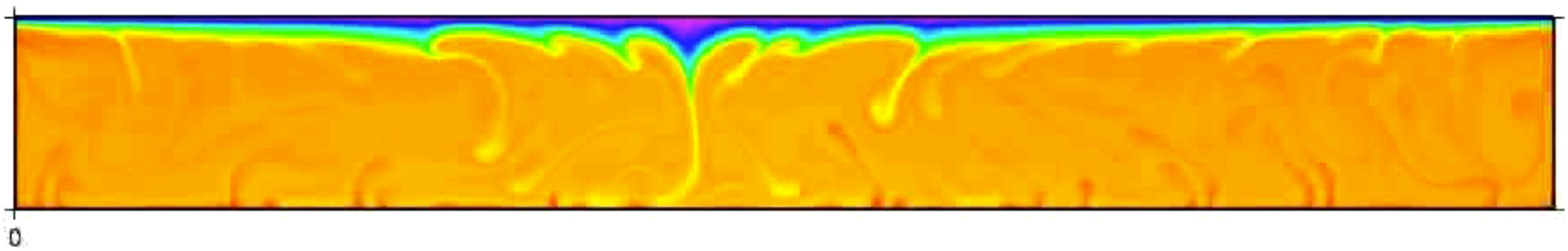

Ra = 1e6

Thermal profiles

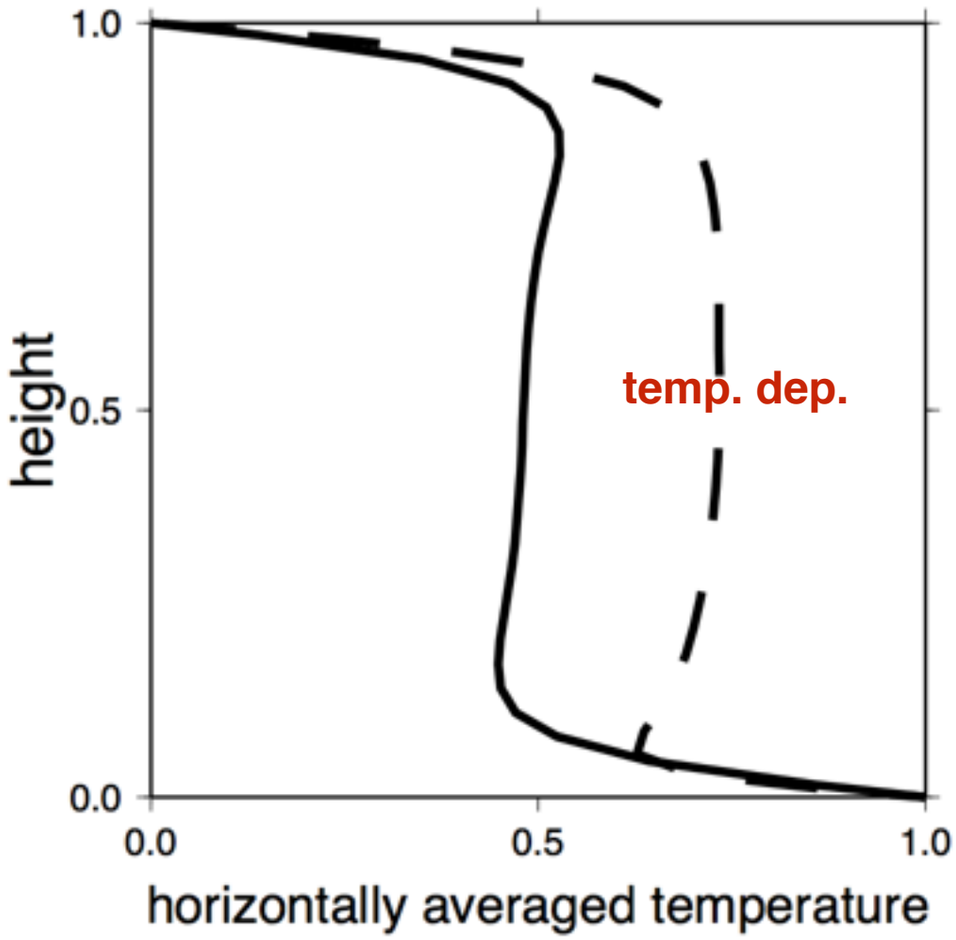

Figure 2. Temperature profiles (i.e., horizontally averaged temperature versus depth) for a basally heated, plane layer of fluid undergoing thermal convection when its viscosity is constant (solid curve) and temperature-dependent (dashed). The profiles show that most of the temperature change across the fluid occurs in relatively narrow *thermal boundary layers* near the top and bottom surfaces. In between the two boundary layers, most of the fluid is stably stratified or (if very well mixed) homogeneous. The fluid with temperature-dependent viscosity develops a stiffer upper thermal boundary layer which acts as a heat plug (i.e., it reduces convection's ability to eliminate heat), causing most of the rest of the fluid to heat up to a larger average temperature. (After Tackley [1996a].)

- Large aspect ratio between thermal boundary layer thickness
- Large viscosity variations in the upper 200 km
- Asymmetry between upwellings and downwellings

(Bercovici, Richard, Richards, GEOPHYSICAL MONOGRAPH, 2000)

Dynamical regimes

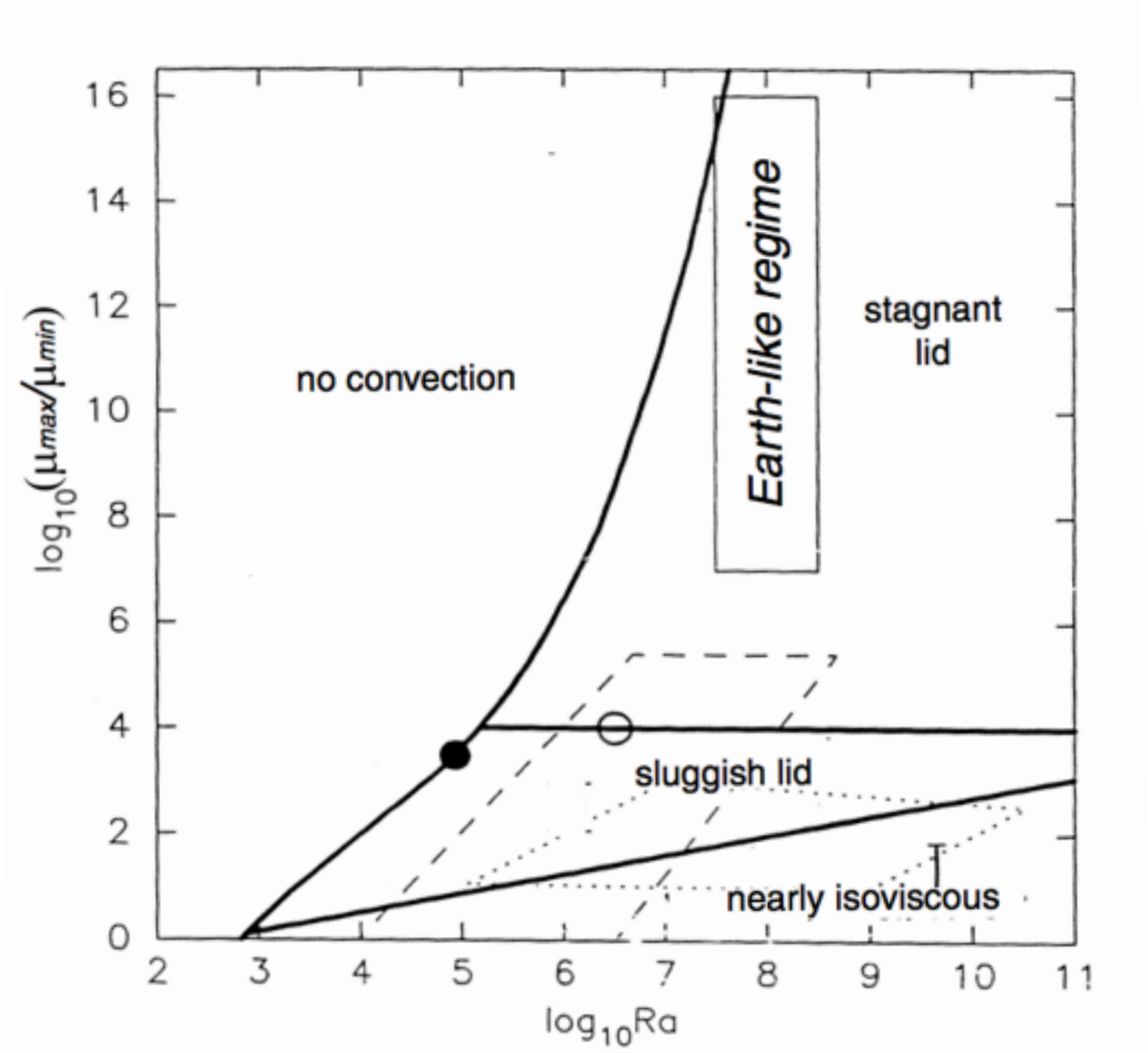

Figure 6. Diagram showing the different convective regimes in "Ra versus viscosity ratio" space for convection in fluid with temperature-dependent viscosity; μ_{max} and μ_{min} are the maximum and minimum allowable viscosities of the fluid, respectively. Dashed and dotted boxes show the regime of various numerical convection experiments. The box with the solid boundary shows the likely regime for the Earth. See text for discussion. (After Solomatov [1995].)

(Bercovici, Richard, Richards, GEOPHYSICAL MONOGRAPH, 2000)

[Pt 5] Non-Newtonian viscosity

$$\mu_{\text{eff}} = \frac{A^{-1/n}}{2\dot{e}^{(n-1)/n}} \exp\left(\frac{H}{nRT}\right) = \frac{1}{2} A^{-1} \tau^{1-n} \exp\left(\frac{H}{RT}\right)$$

- In some ways, results in more "plate" like behaviour for n = 3, …,5
- At modest *Ra*, power-law tends to modify thermo-viscous flow to look like iso-viscous convection
- Large regional variations in flow velocity correspond inversely with large variations in viscosity

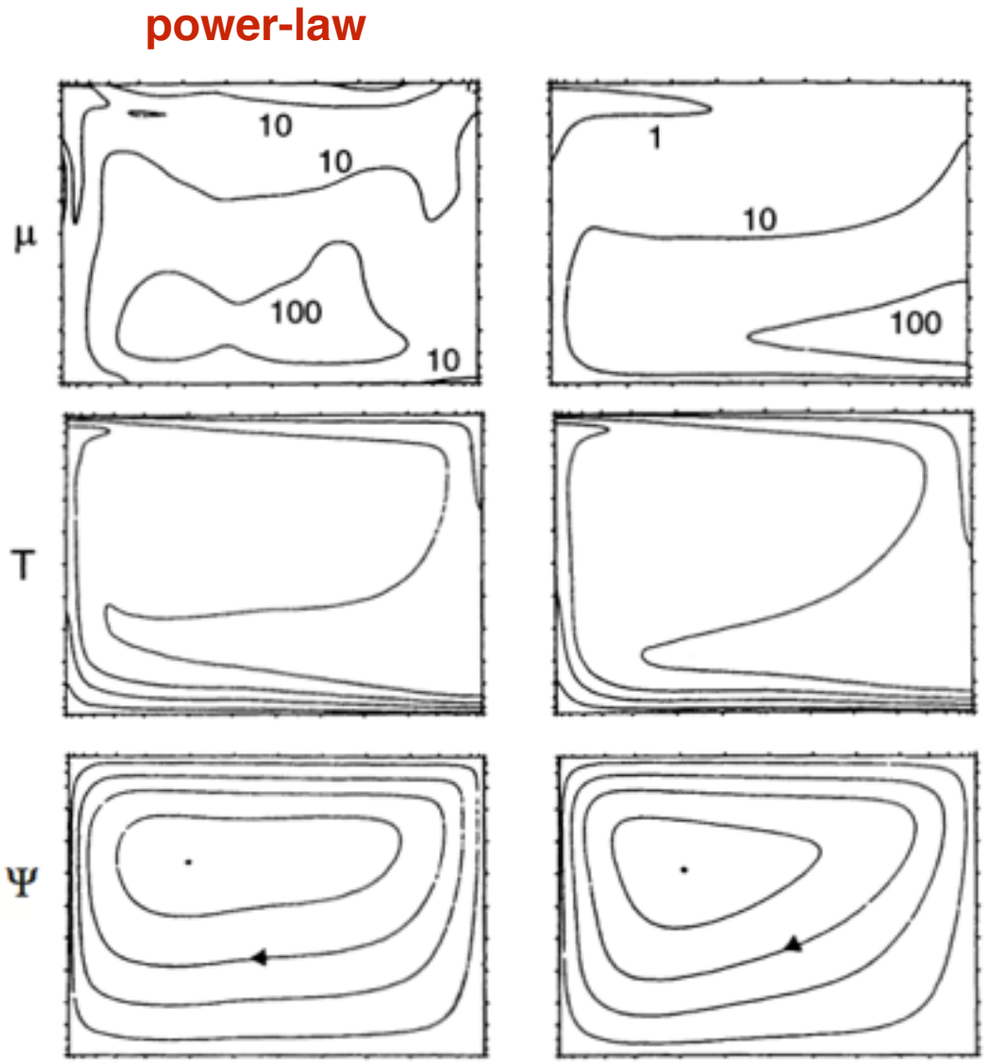

Figure 9.21. A comparison of variable viscosity convection calculations by Christensen (1984a). Left panels illustrate convection in a fluid with non-Newtonian viscosity (power-law exponent $n = 5$) and experimentally determined activation enthalpy for olivine. Right panels show convection in a fluid with Newtonian viscosity and activation enthalpy one-third of the experimentally determined value for olivine. μ is viscosity, T is temperature, and ψ is stream function. Note the logarithmic contour intervals on relative viscosity.

Positive feedback

- Can occur in high Ra systems
- Rapid deformation can lead to very low local viscosities
- Collectively these may couple together to produce small-scale, high velocity upwellings and downwellings

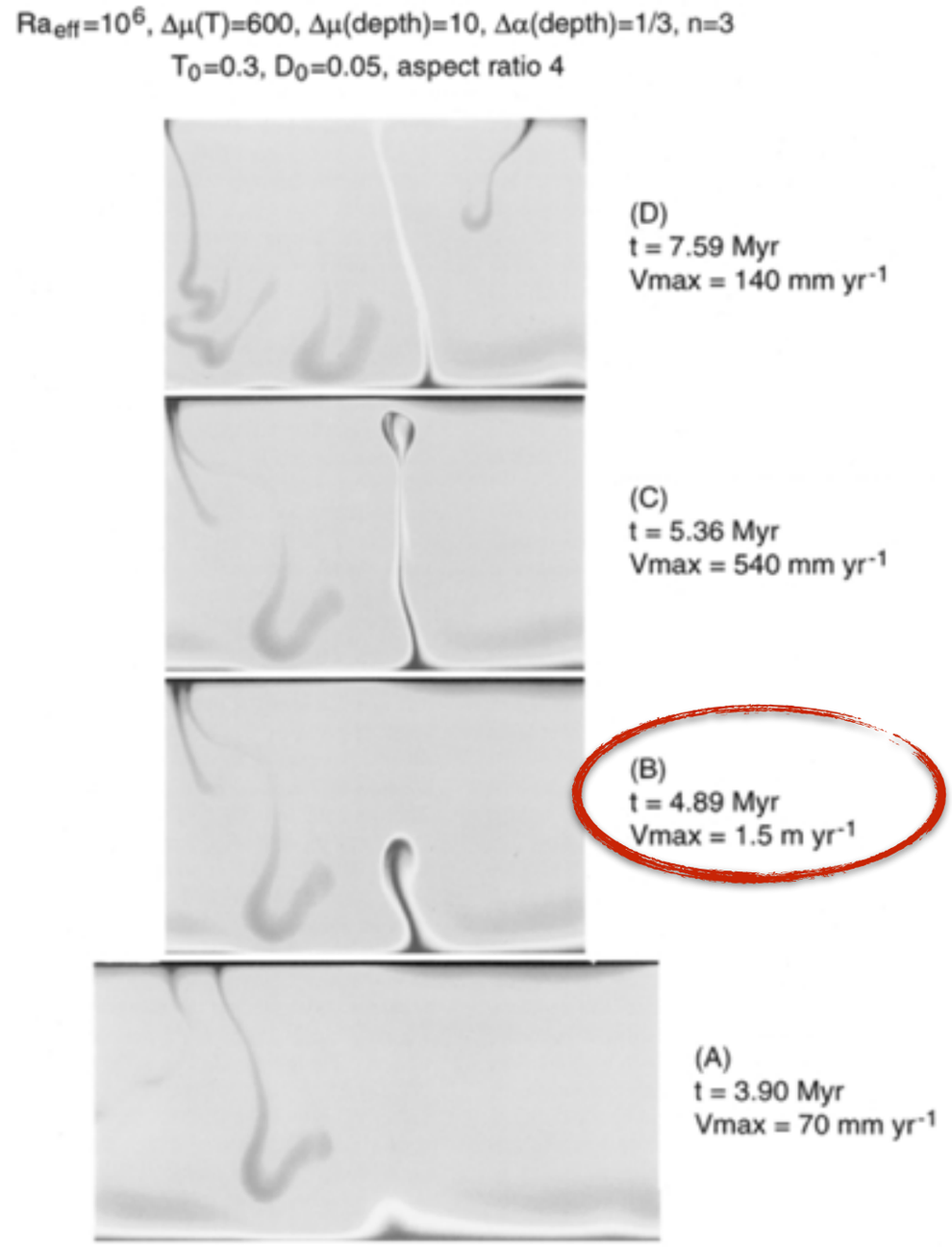

Figure 9.23. Snapshots of temperature showing development of a localized high-velocity upwelling in two-dimensional thermal convection with temperature- and stress-dependent viscosity, from calculations by Larsen and Yuen (1997a). Time increases from bottom to top at approximately 1 Myr intervals. Peak fluid velocities are 0.7, 1.5, 0.54 and 0.14 m yr^{-1}, respectively.

[Pt 6] Rheology with finite yield strength

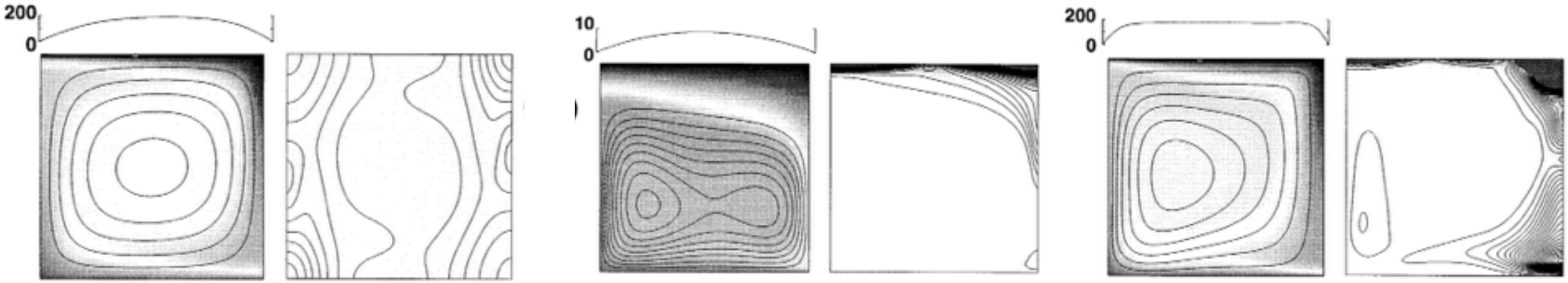

iso-viscous

stagnant lid

plastic
“mobile lid”

$$\eta_{\text{creep}} = \eta_0 \exp(-\theta T)$$

$$\tau_y = c_0 + \phi \rho g z$$

$$\eta_{\text{eff}} = \min\left[\eta_{\text{creep}}, \frac{\tau_y}{2\dot{\epsilon}_{II}}\right]$$

(Moresi & Solomatov, 1998)

Episodic behaviour

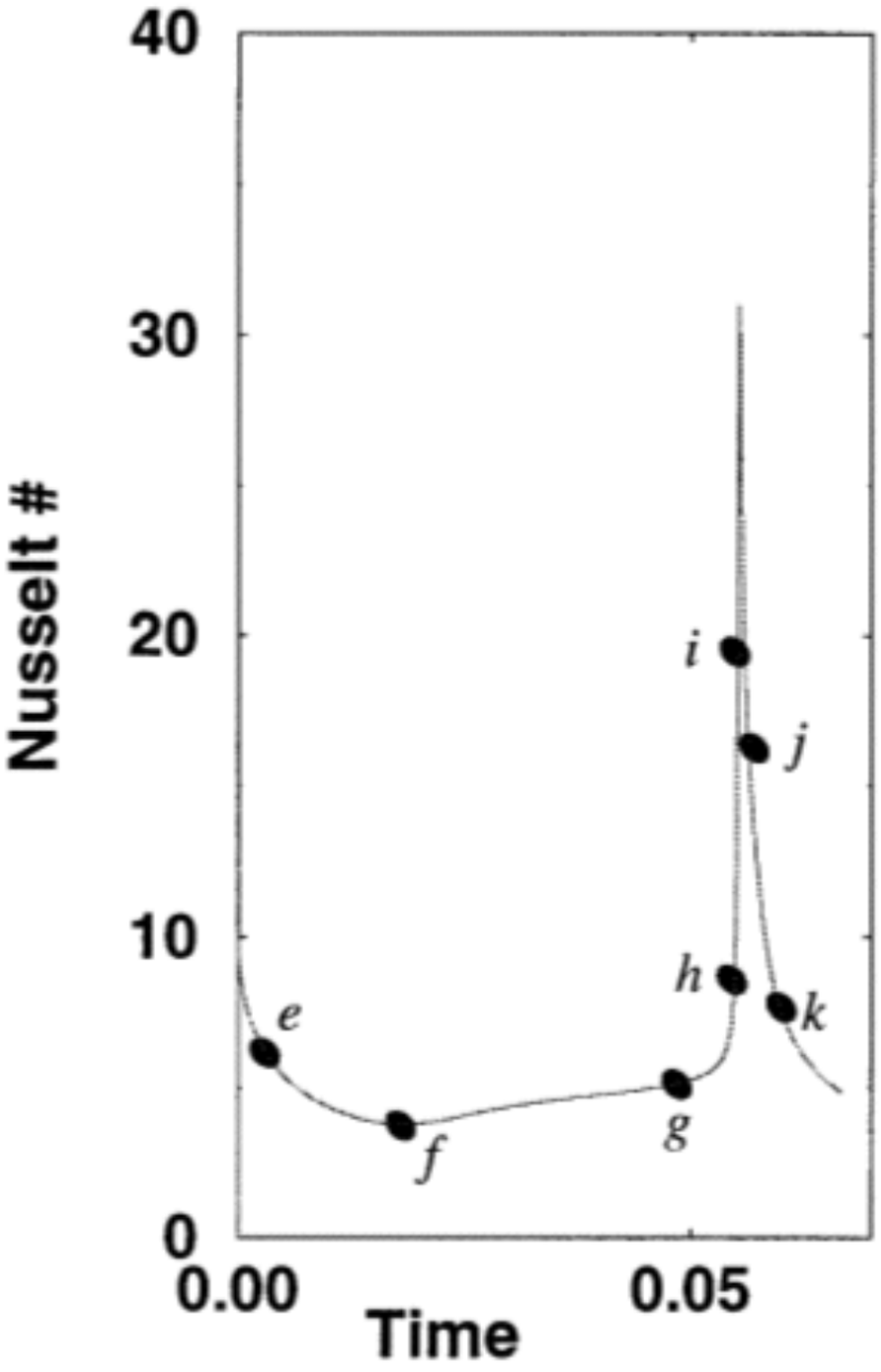

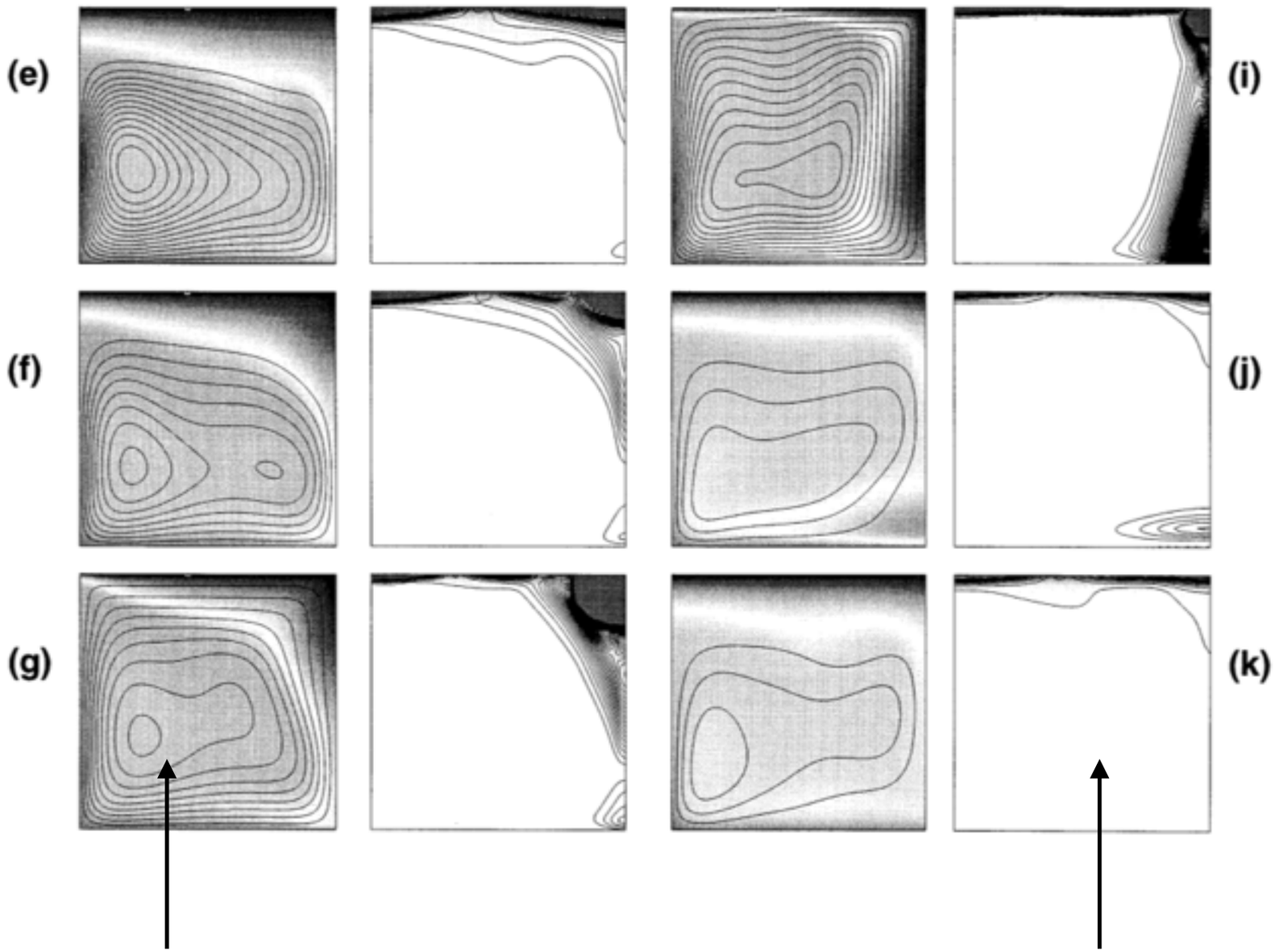

temperature
+ stream lines

stress invariant
contours

Episodic behaviour

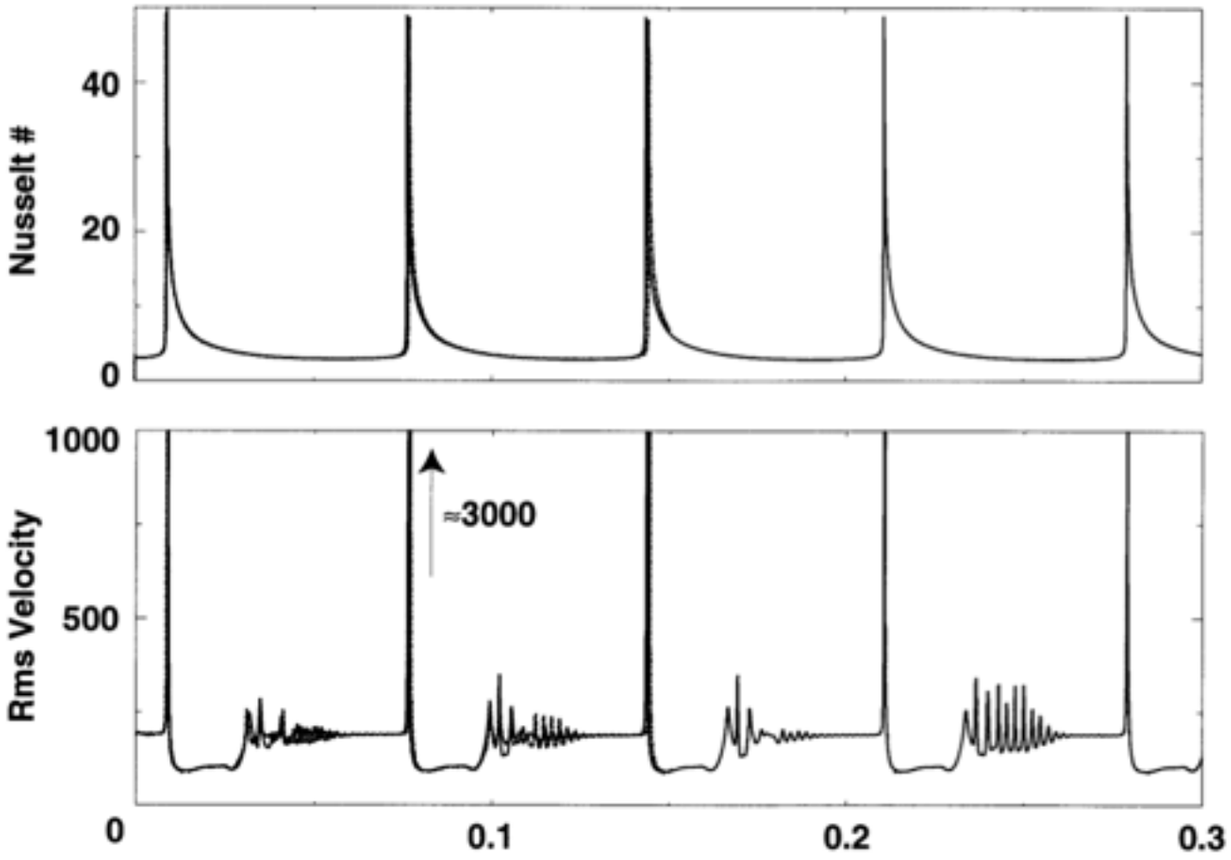

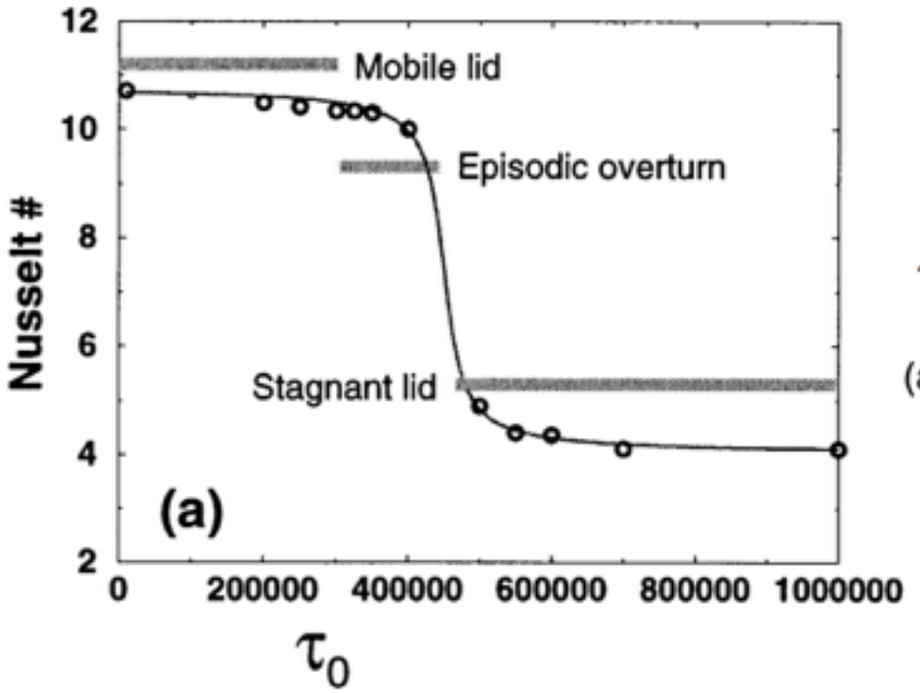

$$\tau'_{\text{yield}} = \tau_0 + \tau_1 z',$$

(a) Ra=10^7 $\Delta\eta$=3x10^4 τ_1=10^7

When the yield stress is high, convection is confined below a thick, stagnant litho-sphere.

At low yield stress, brittle deformation mobilizes the lithosphere which becomes a part of the overall circulation; surface deformation occurs in localized regions close to upwellings and downwellings in the system.

At intermediate levels of the yield stress, there is a cycling between these two states: thick lithosphere episodically mobilizes and collapses into the interior before reforming

[Pt 7] Phase transitions

Clapeyron slope

$$\gamma = \frac{dp}{dT}$$

dp/dT > 0 [exothermic]

$\gamma \sim +1.6$ MPa/K

dp/dT < 0 [endothermic]

$\gamma \sim -2.5$ MPa/K

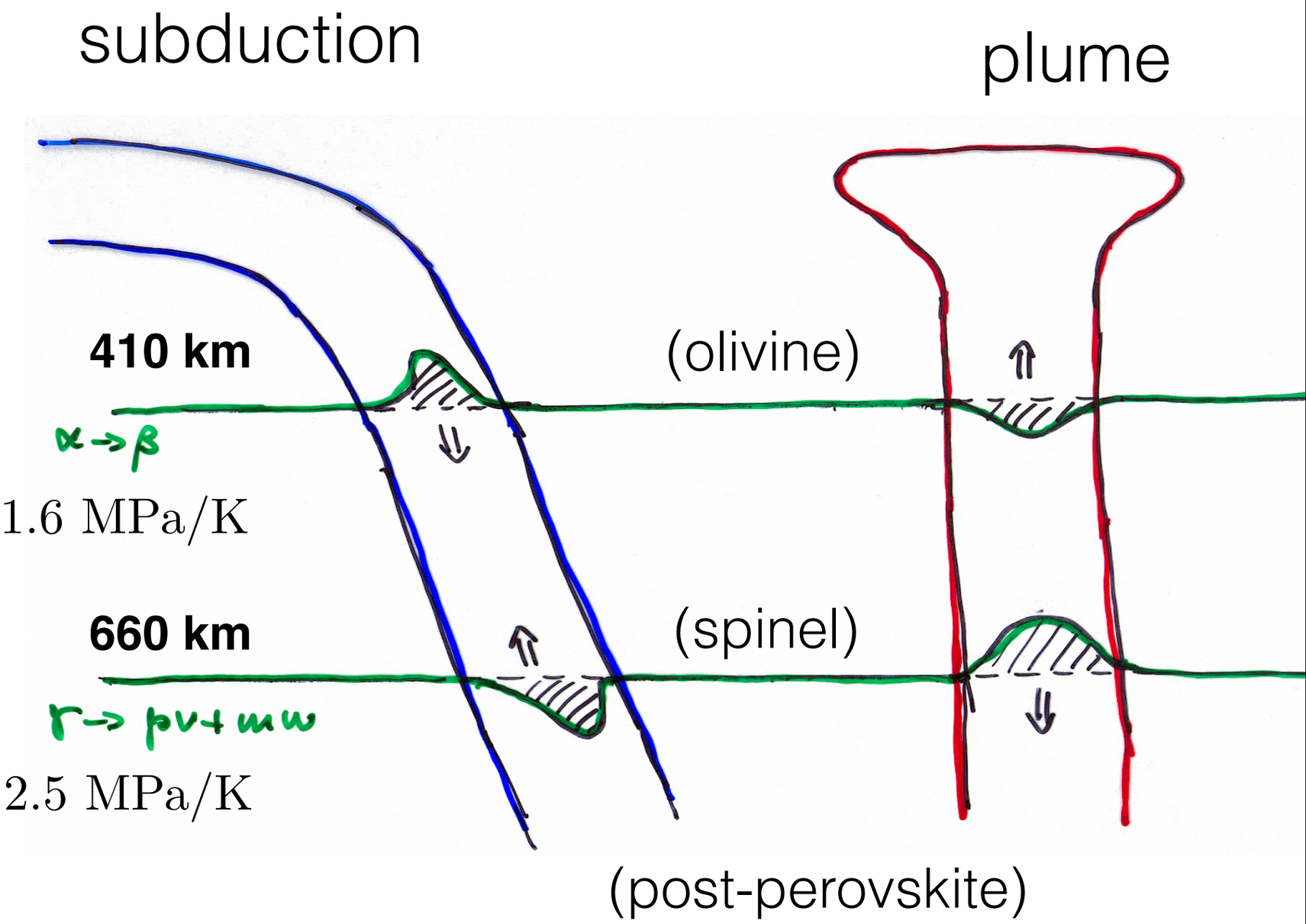

Density of spinel is ~ 280 kg/m3 higher than olivine

Density post-perovskite is ~ 400 kg/m3 higher than spinel

Phase transitions

Clapeyron slope

$$\gamma = \frac{dp}{dT}$$

dp/dT > 0
(exothermic)

dp/dT < 0
(endothermic)

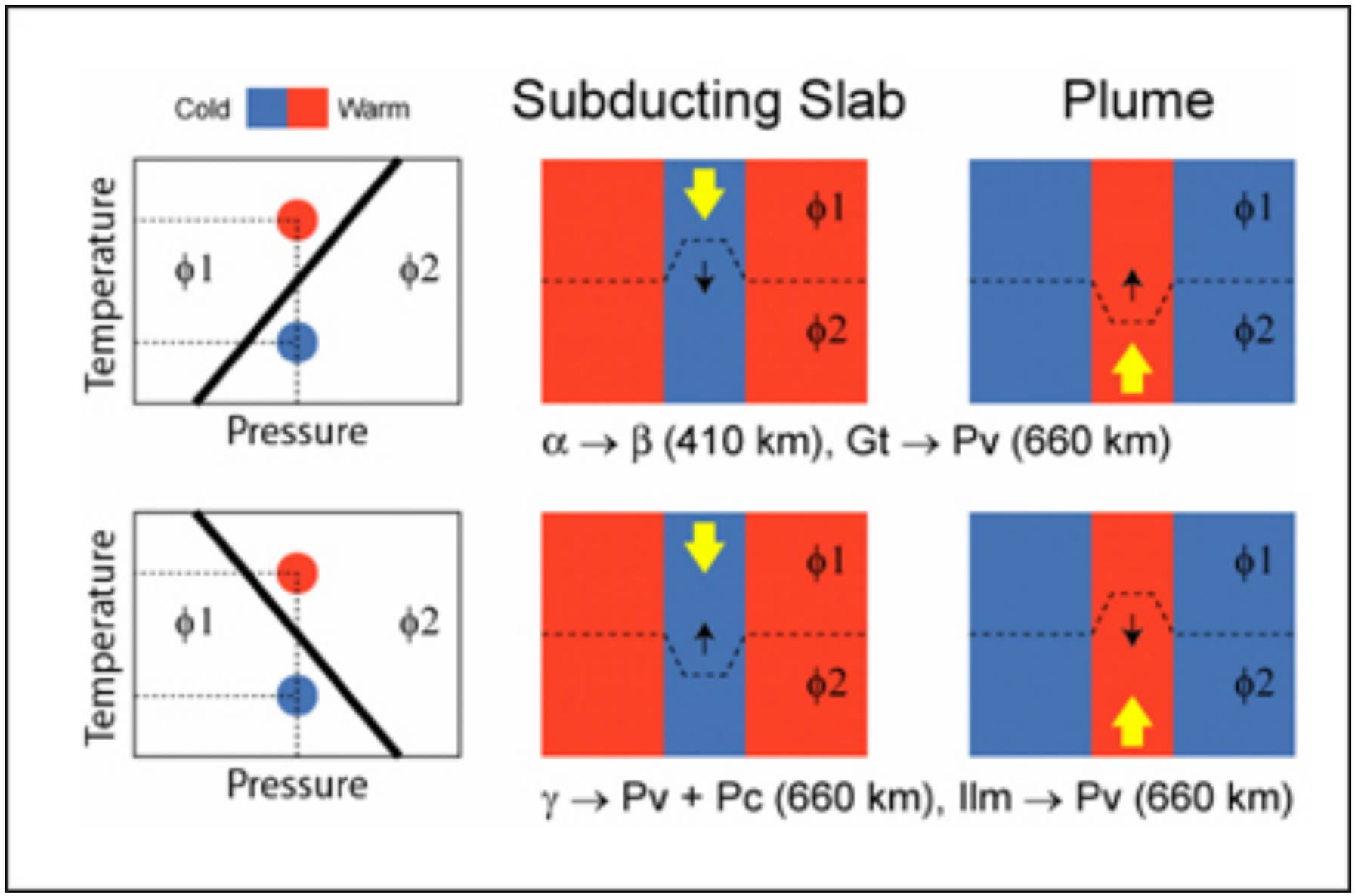

Phase transitions

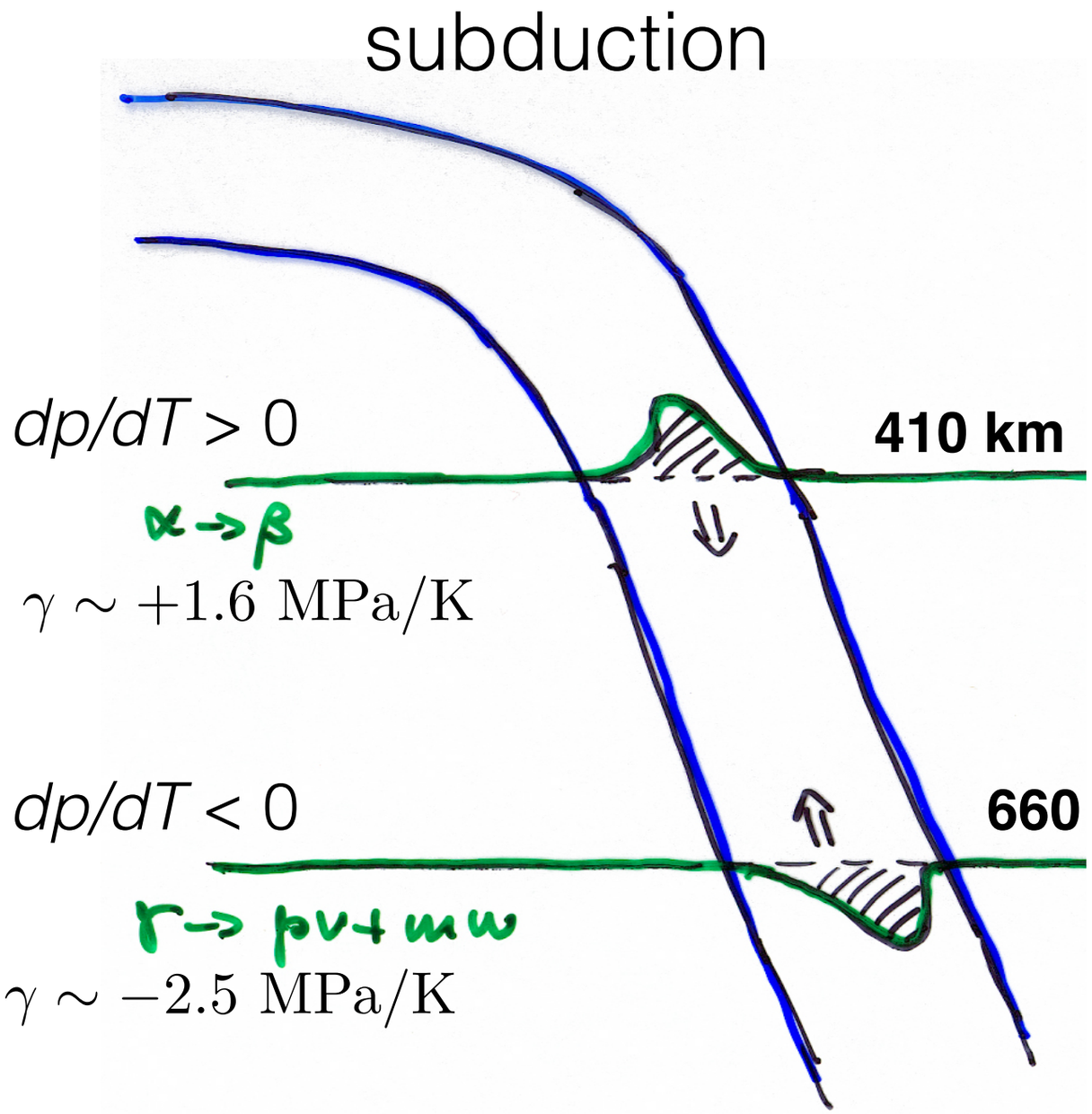

Transition into the denser phase occurs at shallower depths (i.e. lower pressure). Hence, relative to the background mantle, the slab is more negatively buoyant

Transition into the denser phase occurs at much greater depths (i.e. higher pressure). Thus, relative to the background mantle, the negative buoyancy of the slab is reduced, or can in fact become ~ 0.

Phase transitions:Slabs

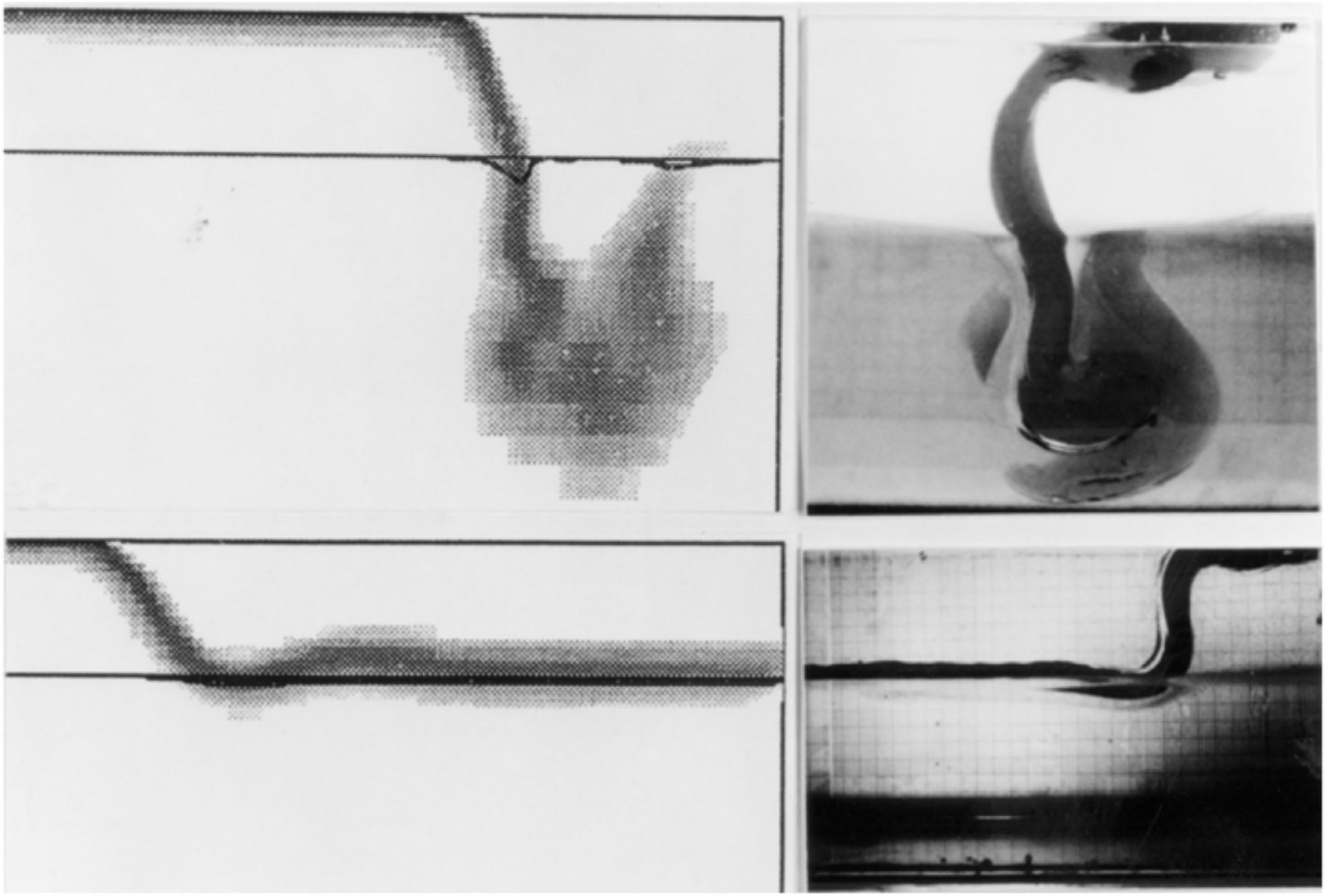

Figure 9.17. Comparison of slab deformation calculated by Christensen (1996; left) with laboratory experiments by Guillou-Frottier et al. (1995; right). Top panels show slab penetration across density and viscosity discontinuities without trench rollback. Bottom panels show slab deflection at the discontinuity with trench rollback.

Phase transitions

Makes convection more episodic

Periods of two-layer convection, followed by whole-mantle convection

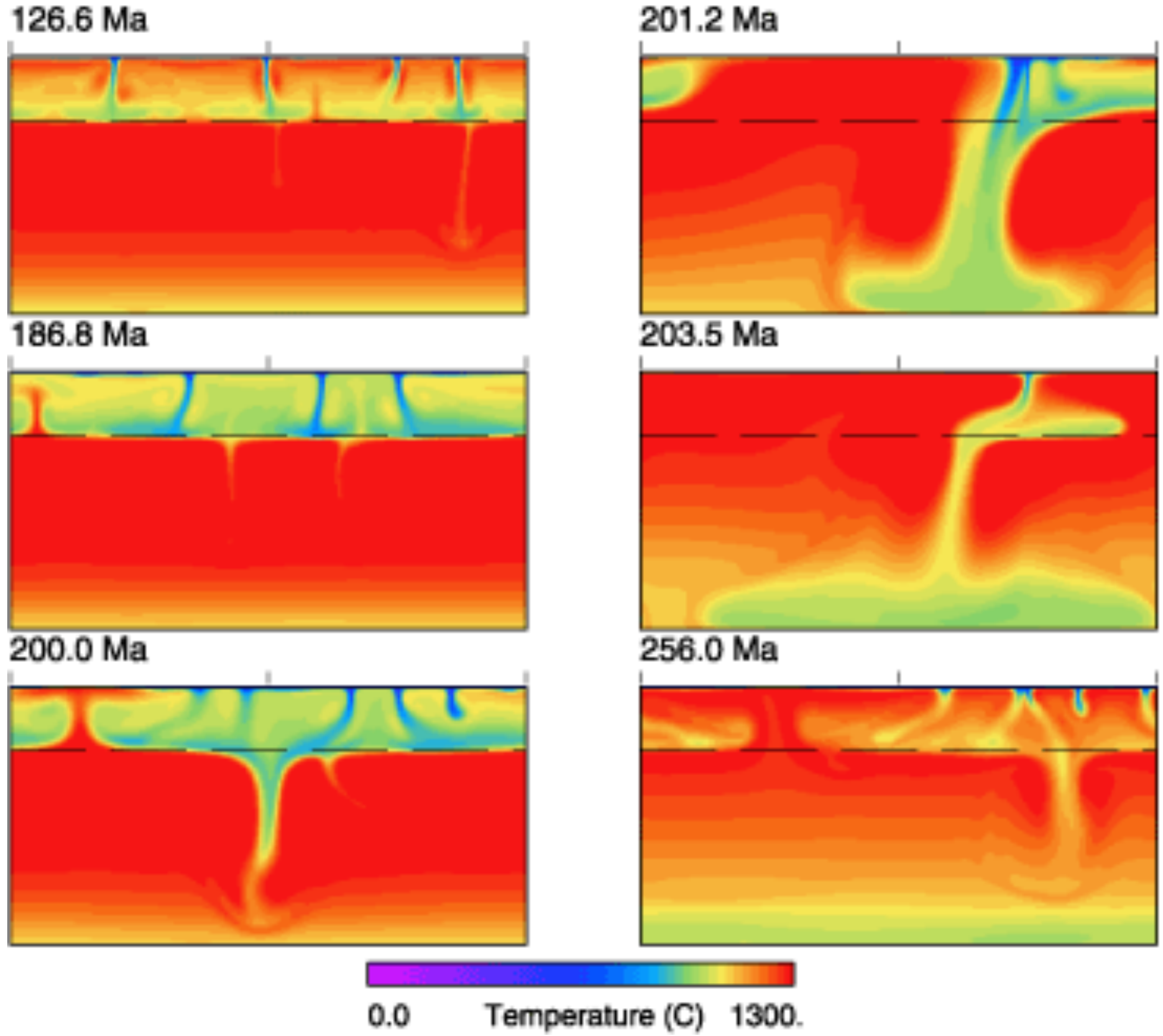

(Davies, 1995)

Phase transitions

The strength of the slab is important

Strong slabs may penetrate, weak slabs may founder

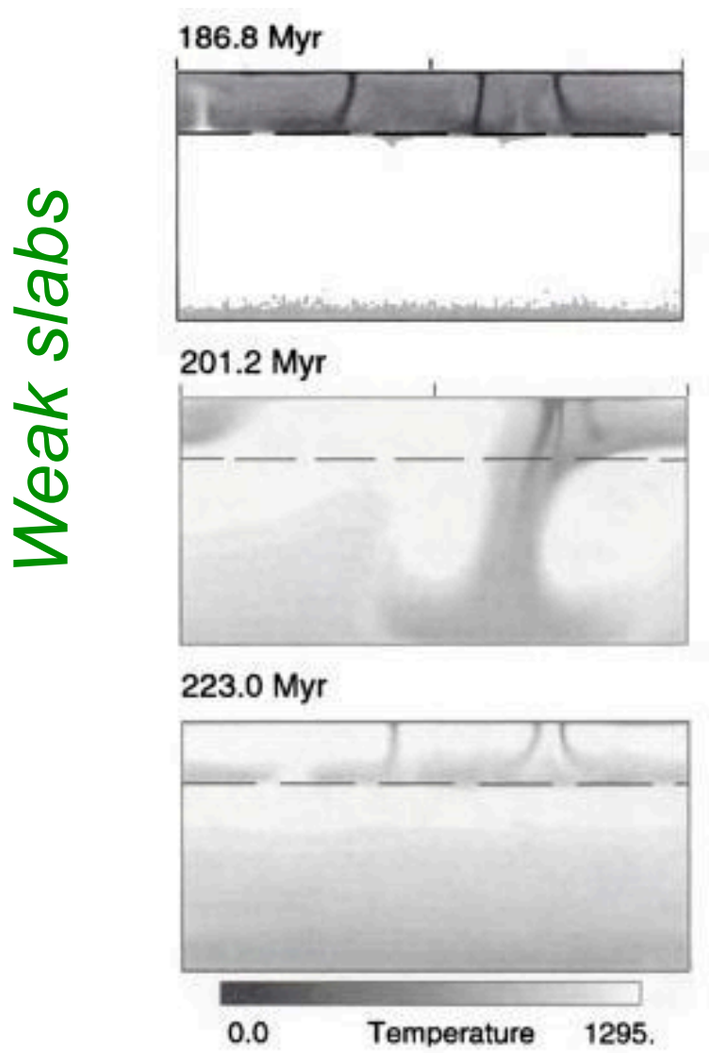

Figure 5.4. Sequence from a numerical convection model with constant viscosity showing transient layering and an overturn event. The buoyancy from a phase transformation with a Clapeyron slope of −3 MPa/°C is included at the depth of the dashed line.

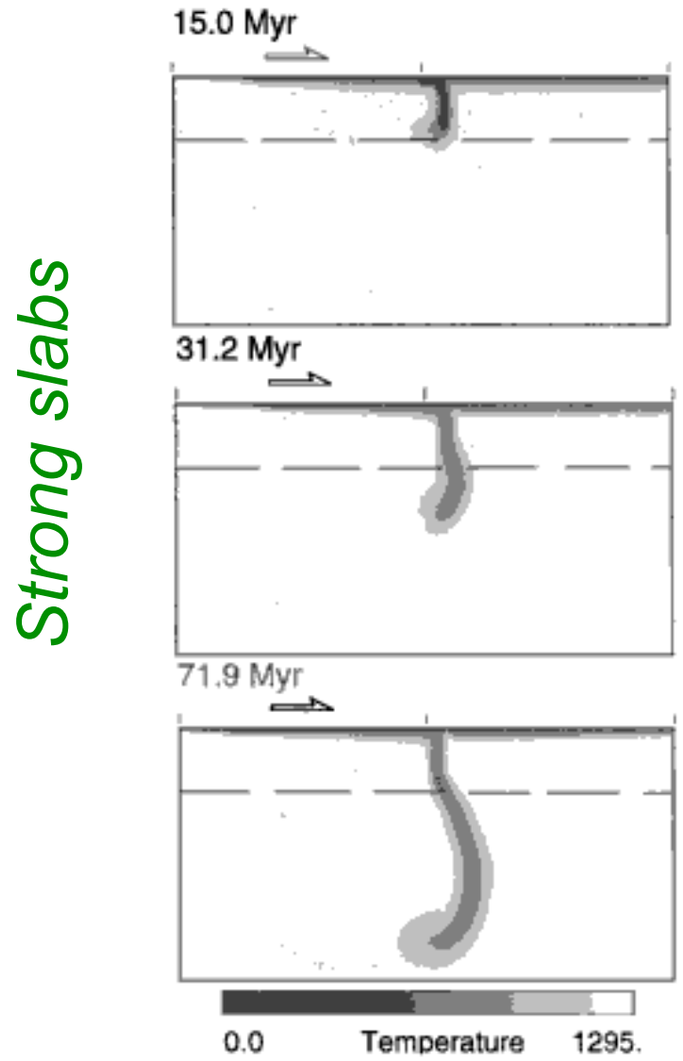

Figure 5.5. Sequence from a numerical convection model with stiff, but mobile, plates. The viscosity is temperature-dependent, with a maximum viscosity at the cold surface 200 times the viscosity of the interior. Also, the viscosity is reduced locally at each end of the mobile plate, allowing it to move. Phase-transformation buoyancy with a Clapeyron slope of −3 MPa/°C is included. The thicker, stronger slab is able to penetrate the phase barrier, whereas the constant-viscosity downwellings of Figure 5.4 did not.

Phase transitions: Plumes

The magnitude of the Clapeyron slope is important for mantle plume migration

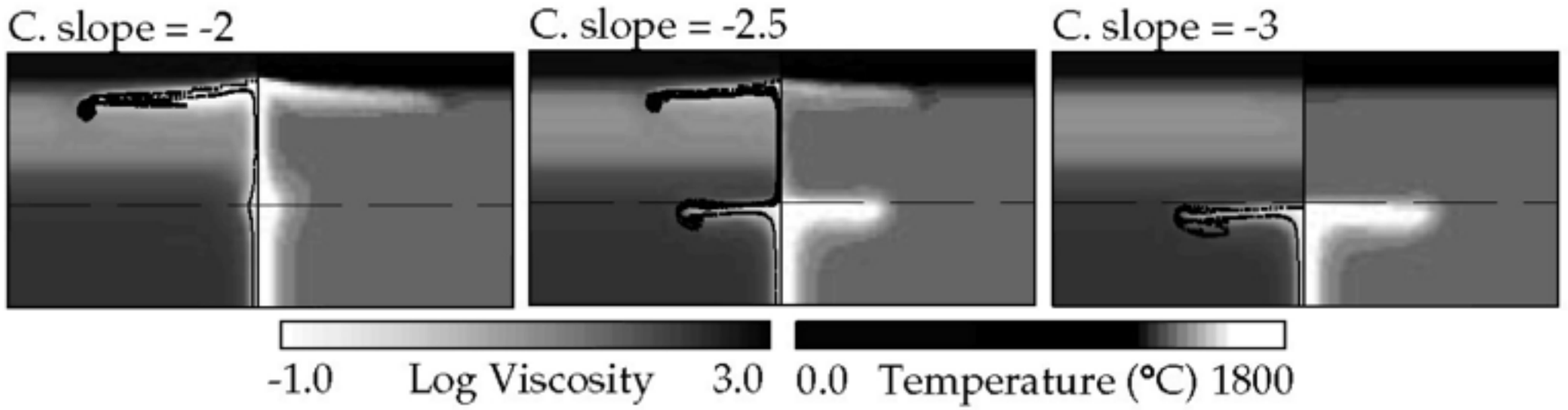

Figure 11.11. Plume models like that in Figure 11.10, but with different Clapeyron slopes (C. slope) of the phase transformation. The viscosity structure is shown on the left of these panels and the temperature on the right. From Davies [27]. Copyright by Elsevier Science. Reprinted with permission.

Phase transitions

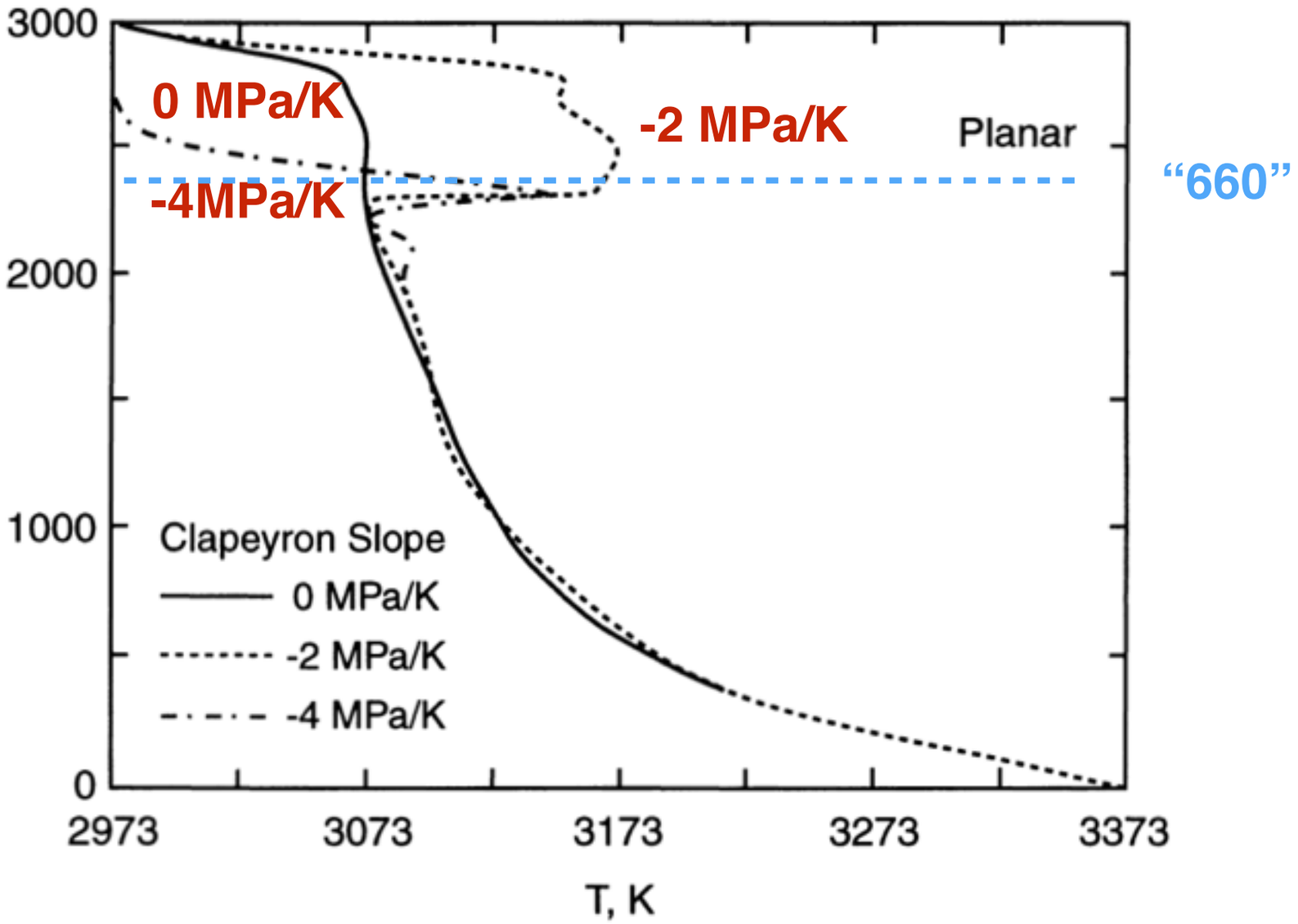

Figure 9.20. Plume centerline temperature as a function of height above the lower boundary in the numerical model of Schubert et al. (1995). Plumes encounter an endothermic phase change 660 km below the top boundary with Clapeyron slopes of 0, −2, −4 MPa K^{-1}. The case of a Clapeyron slope of 0 MPa K^{-1} is equivalent to no phase change. For a Clapeyron slope of −2 MPa K^{-1} the plumes penetrate the phase change, but for a slope of −4 MPa K^{-1} they are stopped by the phase change. Passage through the phase change (−2 MPa K^{-1}) results in considerable heating of the plume (compare with 0 MPa K^{-1}). Axisymmetric plumes are hotter than planar plumes although both start out at the same temperature at the lower boundary.

Phase transitions

- Results depend on Clapeyron slope and nature of anomaly (slab “cold” versus plume “hot”)
- Christensen & Yuen (1985) indicate layered convection occurs if the slope is steeper than -6 MPa/K
- Chemical differences between upper and lower mantle can change the regime
- Strength of slabs and chemical heterogeneity with the slab can influence the regime
- New laboratory results favour smaller Clapeyron slope

[Pt 8] Compositional variations

$$-\nabla p + \eta \nabla^2 \boldsymbol{v} = \boldsymbol{f}$$

$$\boldsymbol{f} = \left(\Delta\rho_{\text{composition}} - \rho_0 \alpha \Delta T\right) g \hat{\boldsymbol{e}}_z$$

chemically distinct materials

thermal contraction/expansion

Buoyancy number

$$B = \frac{\delta\rho_{\text{composition}}}{\rho_0 \alpha \Delta T}$$

- buoyancy from composition / Boussinesq

Compositional variations

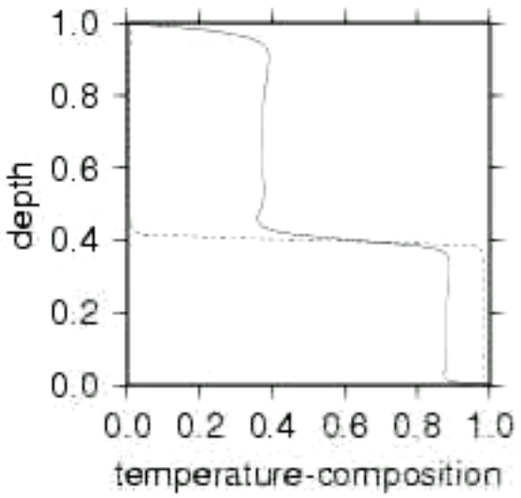

$$Ra = 10^6$$

$$\frac{\eta_{\max}}{\eta_{\min}} = 10^4$$

$$B = 2$$

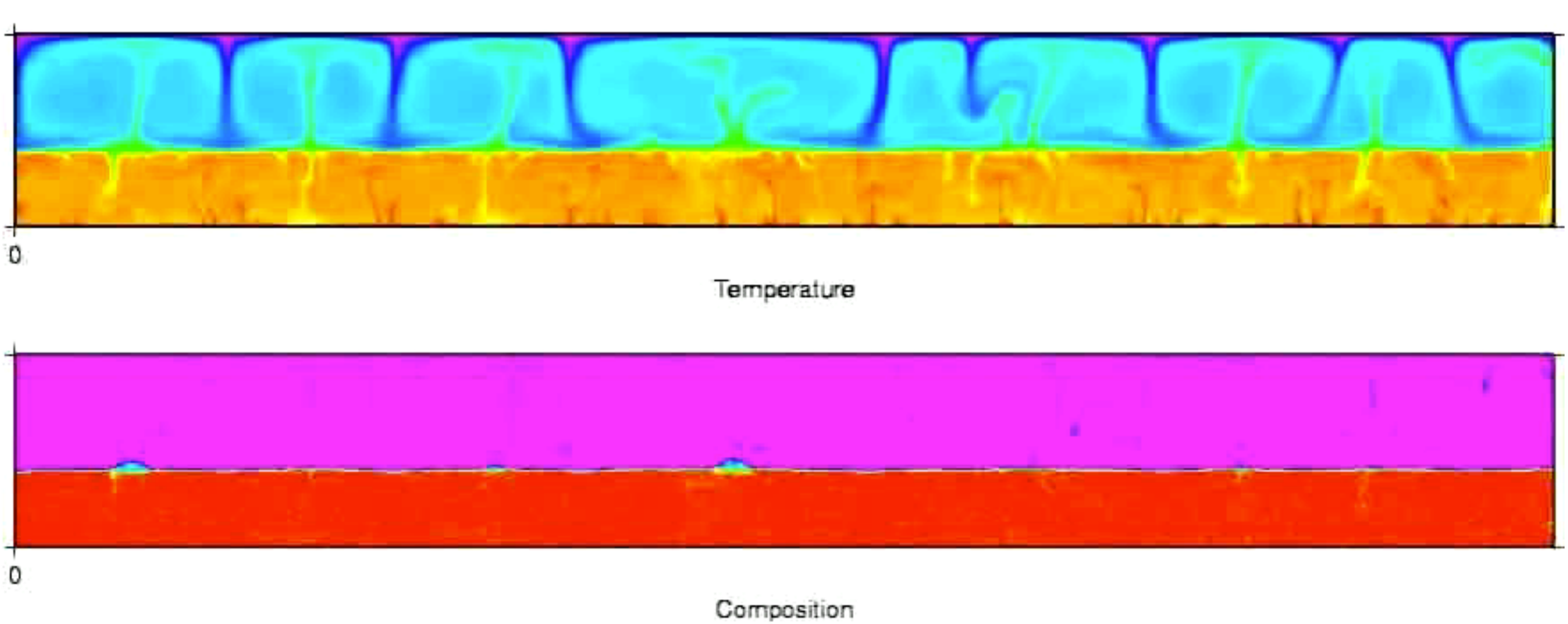

Compositional variations

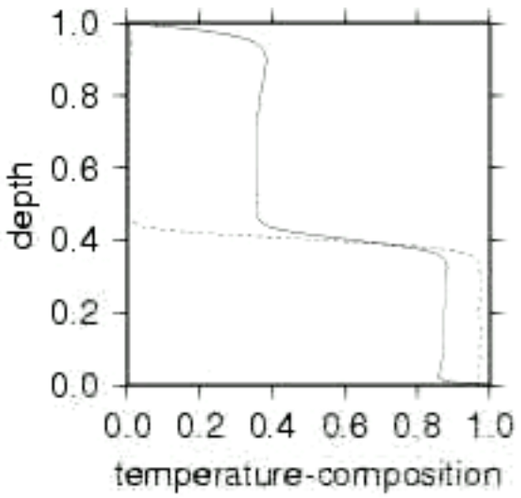

$$Ra = 10^6$$

$$\frac{\eta_{\max}}{\eta_{\min}} = 10^4$$

$$B = 0.8$$

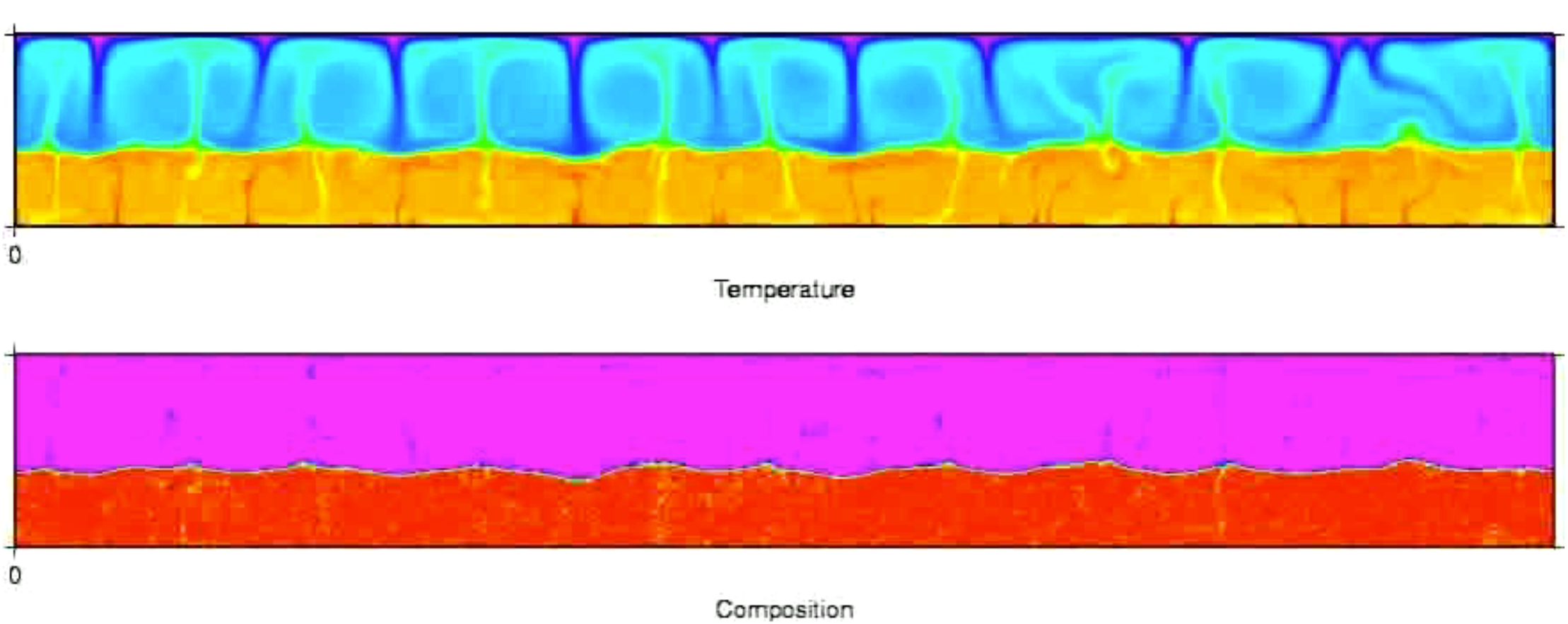

Compositional variations

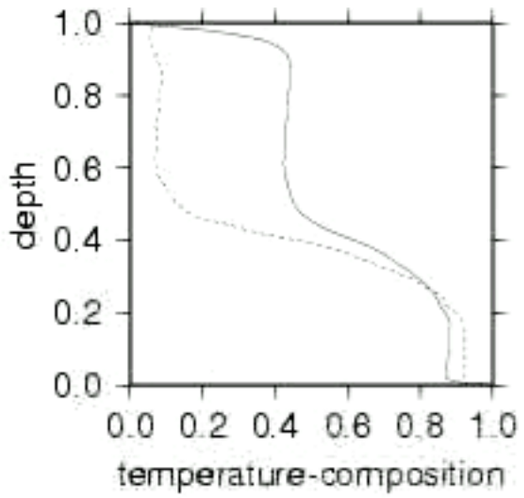

$$Ra = 10^6$$

$$\frac{\eta_{\max}}{\eta_{\min}} = 10^4$$

$$B = 0.6$$

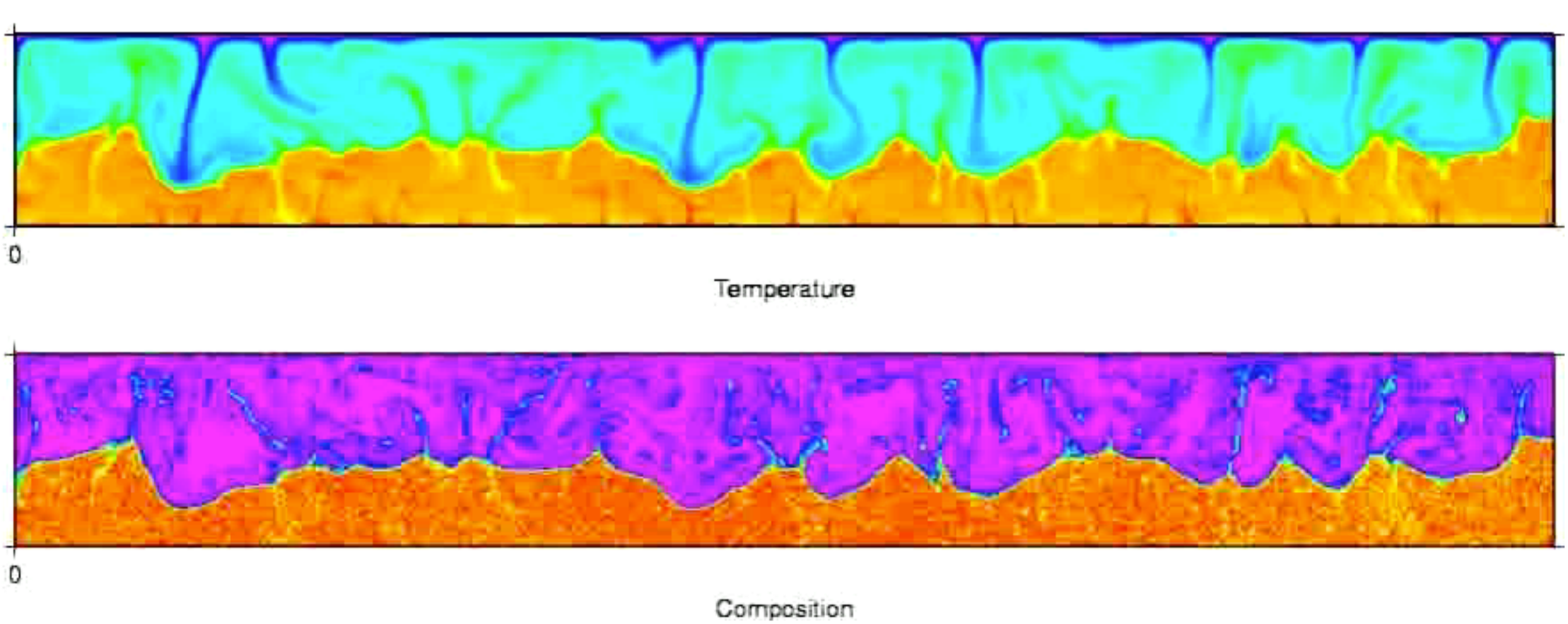

Compositional variations

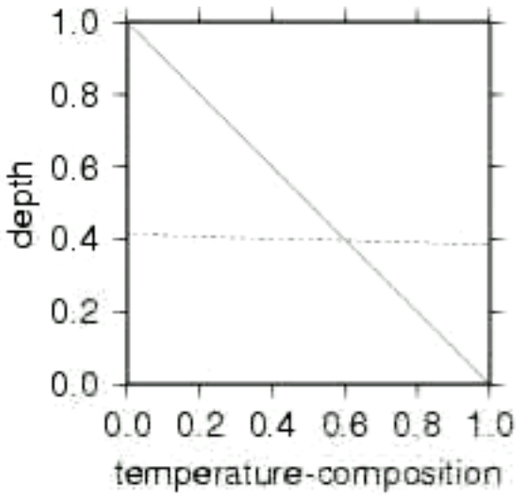

$$Ra = 10^6$$

$$\frac{\eta_{\max}}{\eta_{\min}} = 10^4$$

$$B = 0.5$$

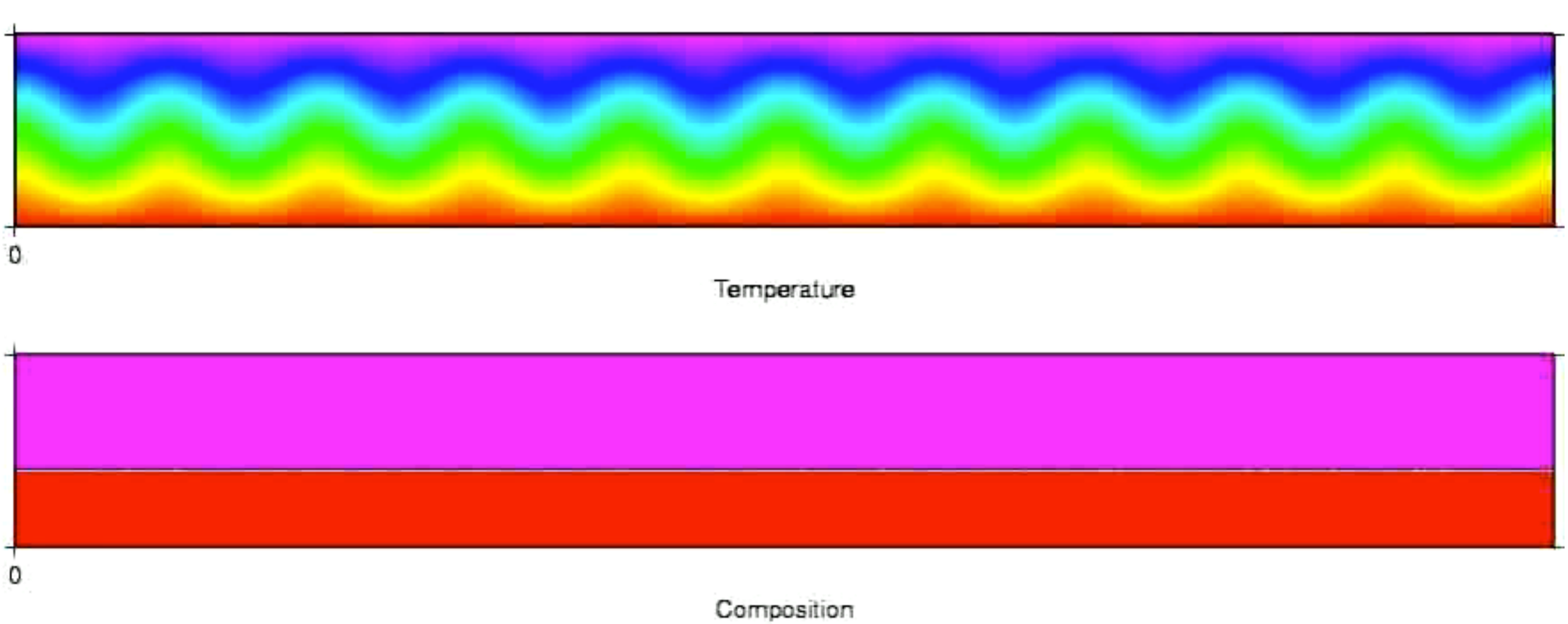

[Pt 9] Role of boundary condition

Why is terrestrial subduction one-sided?

Taras V. Gerya, James A.D. Connolly — Department of Earth Sciences, Swiss Federal Institute of Technology (ETH - Zürich), CH-8092 Zürich, Switzerland
David A. Yuen — University of Minnesota Supercomputing Institute and Department of Geology and Geophysics, University of Minnesota, Minneapolis, Minnesota 55455-0219, USA

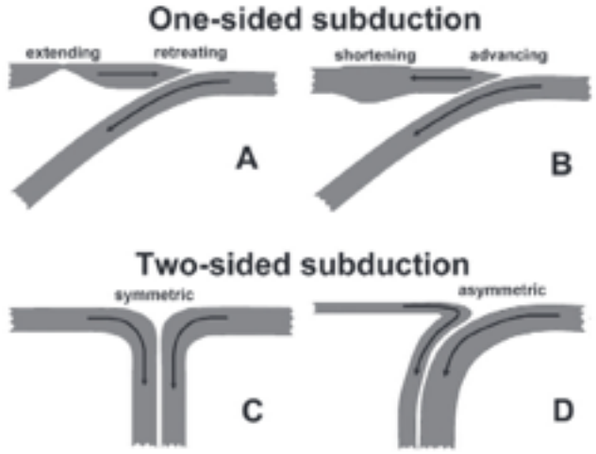

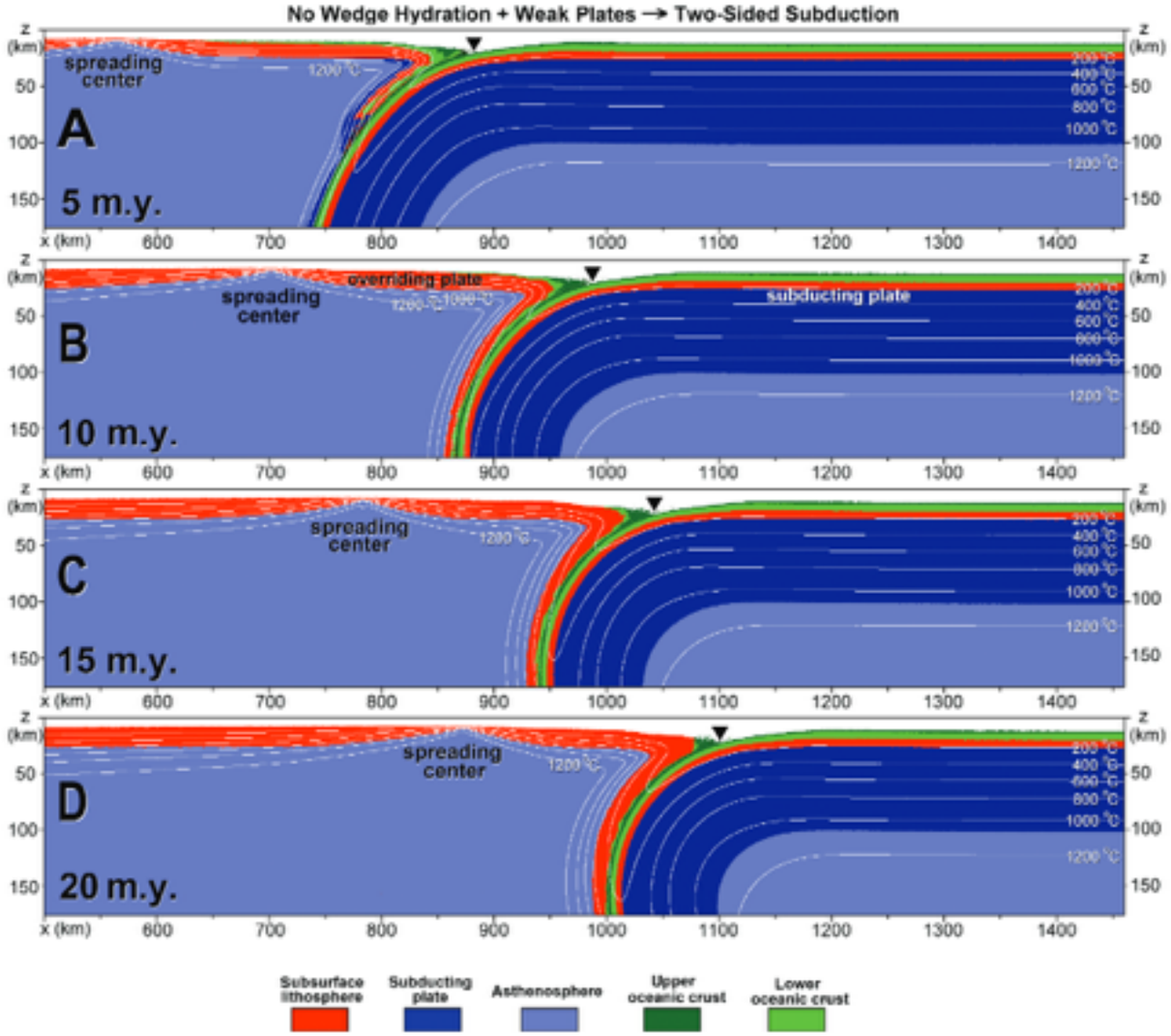

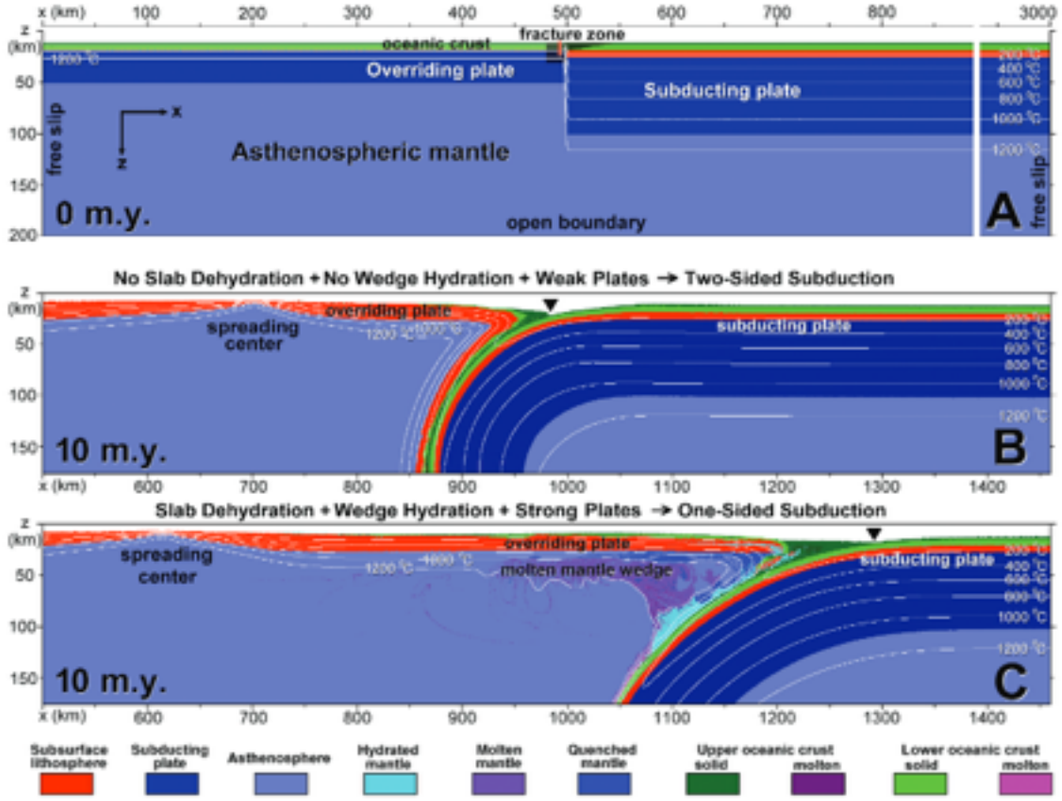

(Gerya et al, *Geology*,2008)

Role of boundary condition

A free plate surface and weak oceanic crust produce single-sided subduction on Earth

F. Crameri,[1] P. J. Tackley,[1] I. Meilick,[1] T. V. Gerya,[1] and B. J. P. Kaus[1,2]

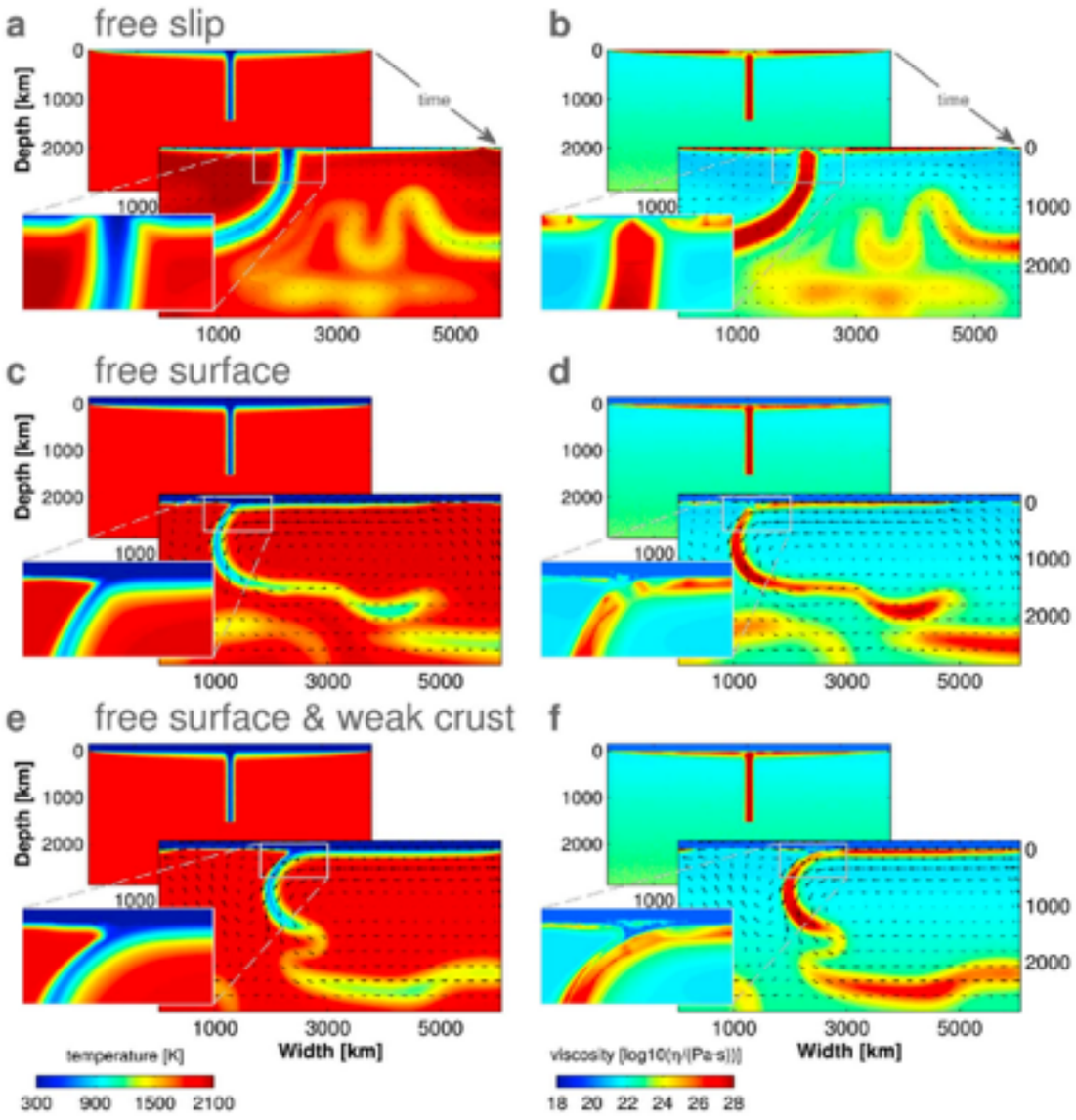

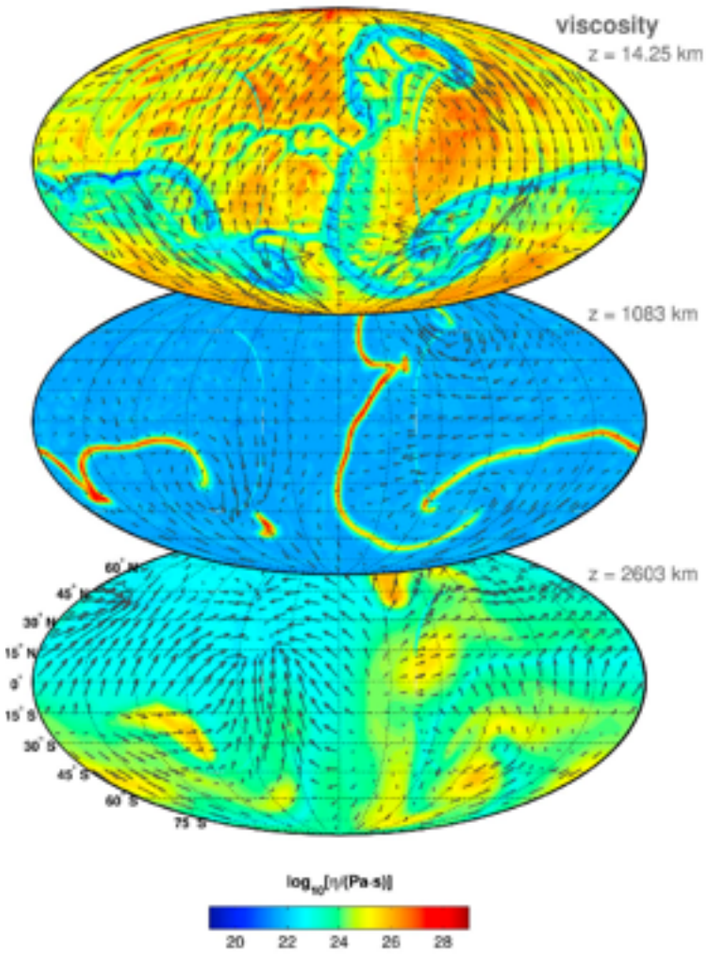

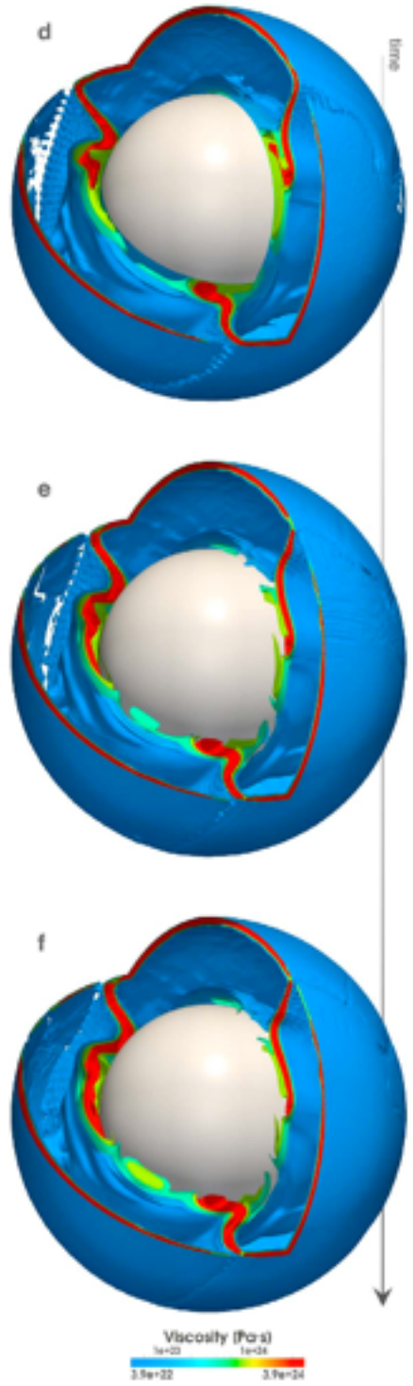

(Crameri, *GRL*,2012)

[Pt 10] Three-dimensionality

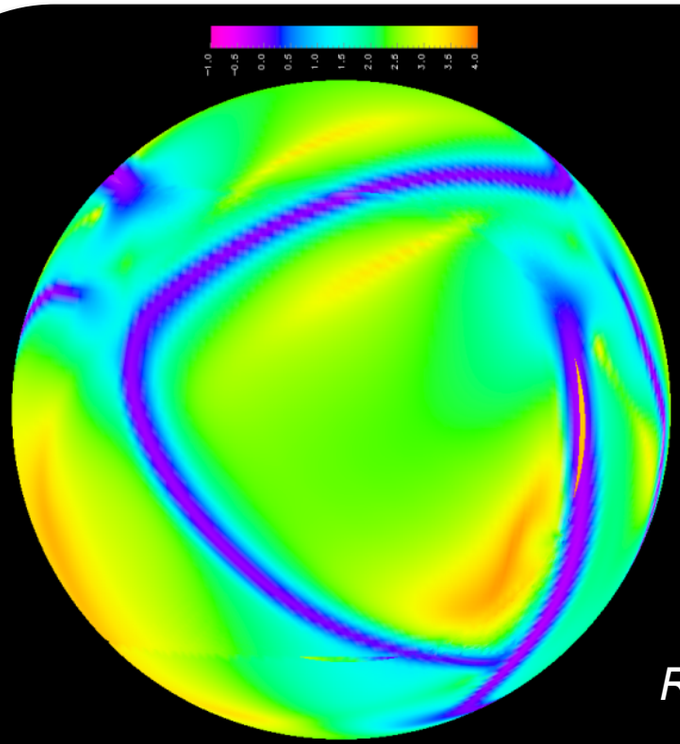

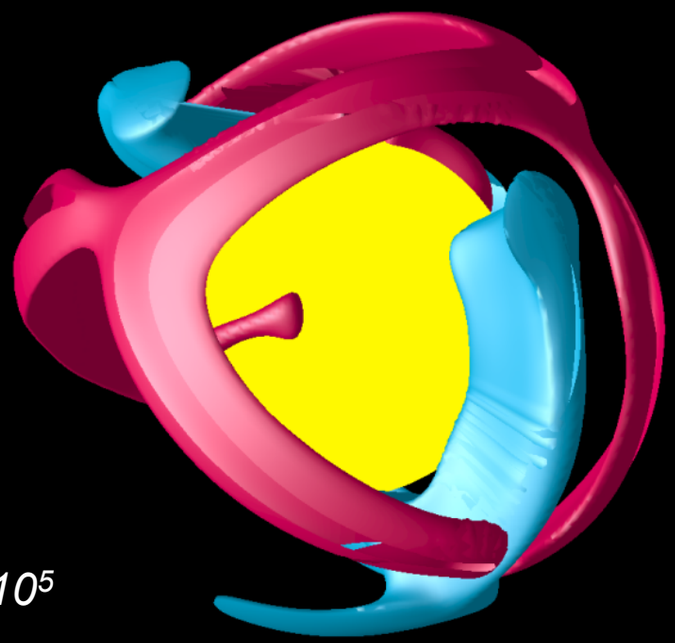

Hein van Heck

Ra=10⁵

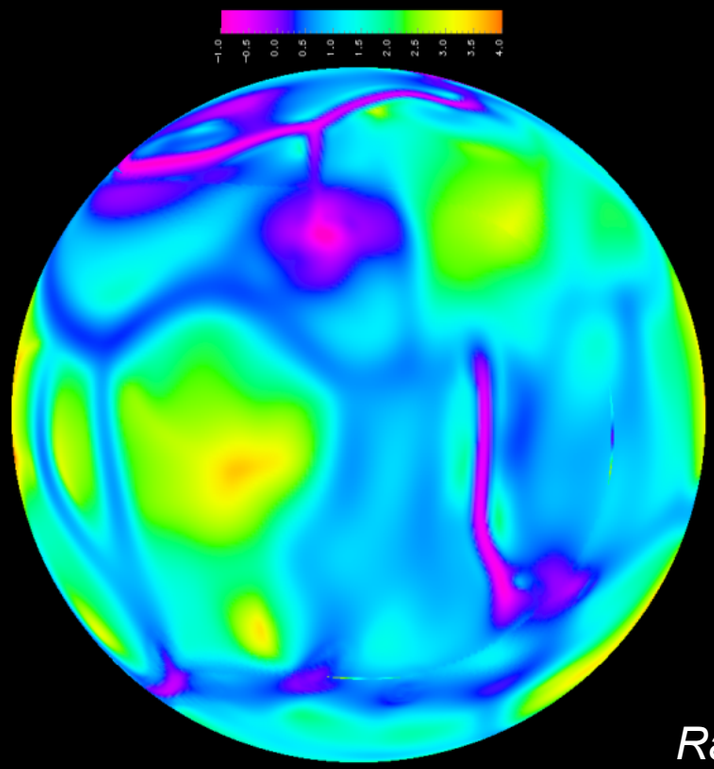

Ra=10⁵

[Pt 10] Three-dimensionality

Ra = 1e7
Bottom heated,
$H = 20$

Less upwellings as before

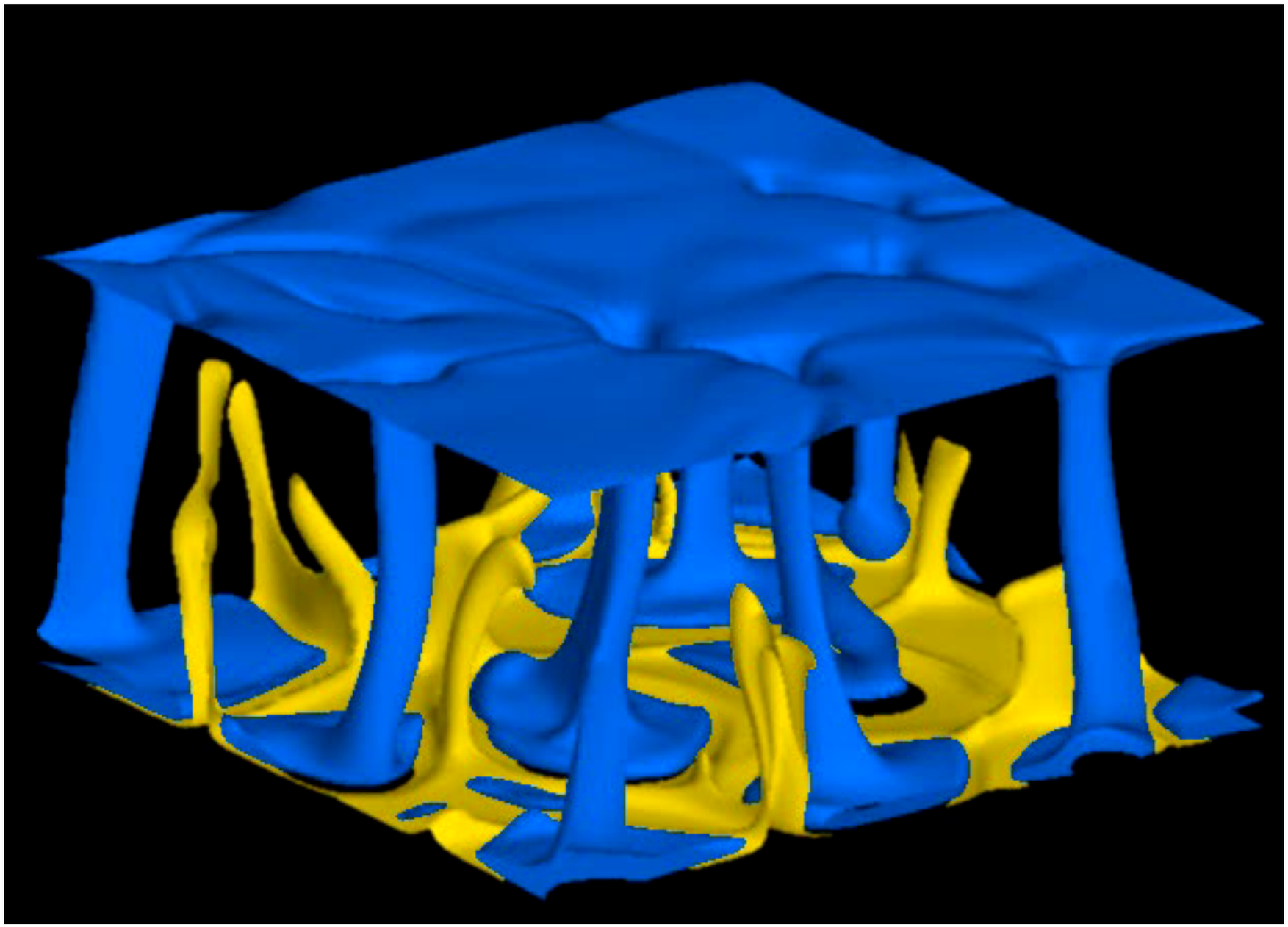

Compressible, viscosity increases with depth, phase transition at 660 km

Ra = 2e6

Ra = 1e7

Ra = 4e7

Ra = 6e7

Ra = 1e8

Ra = 4e8

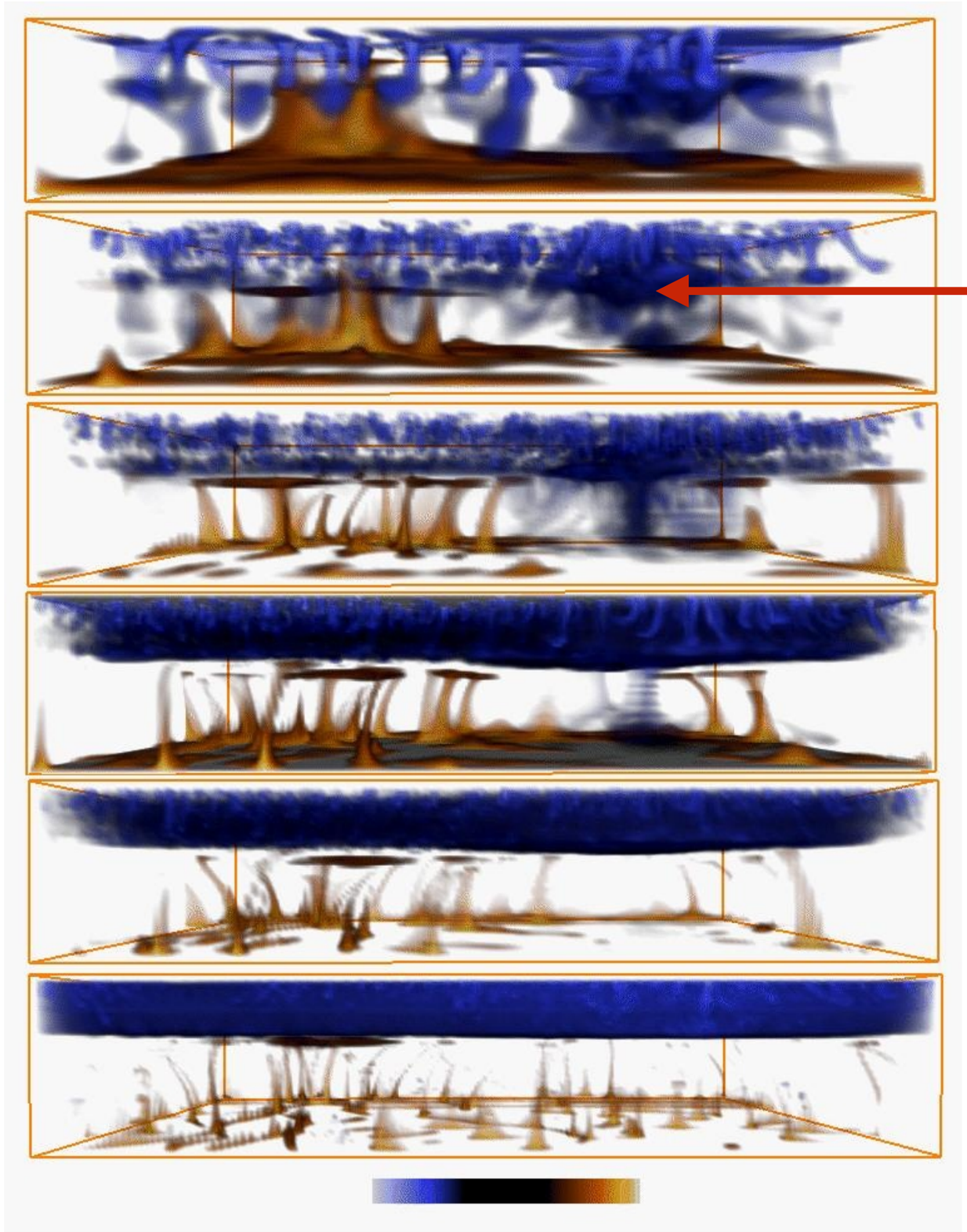

Avalanches into lower mantle

Mantle becomes more stratified

Completely layered convection

(Yuen et al,1994)

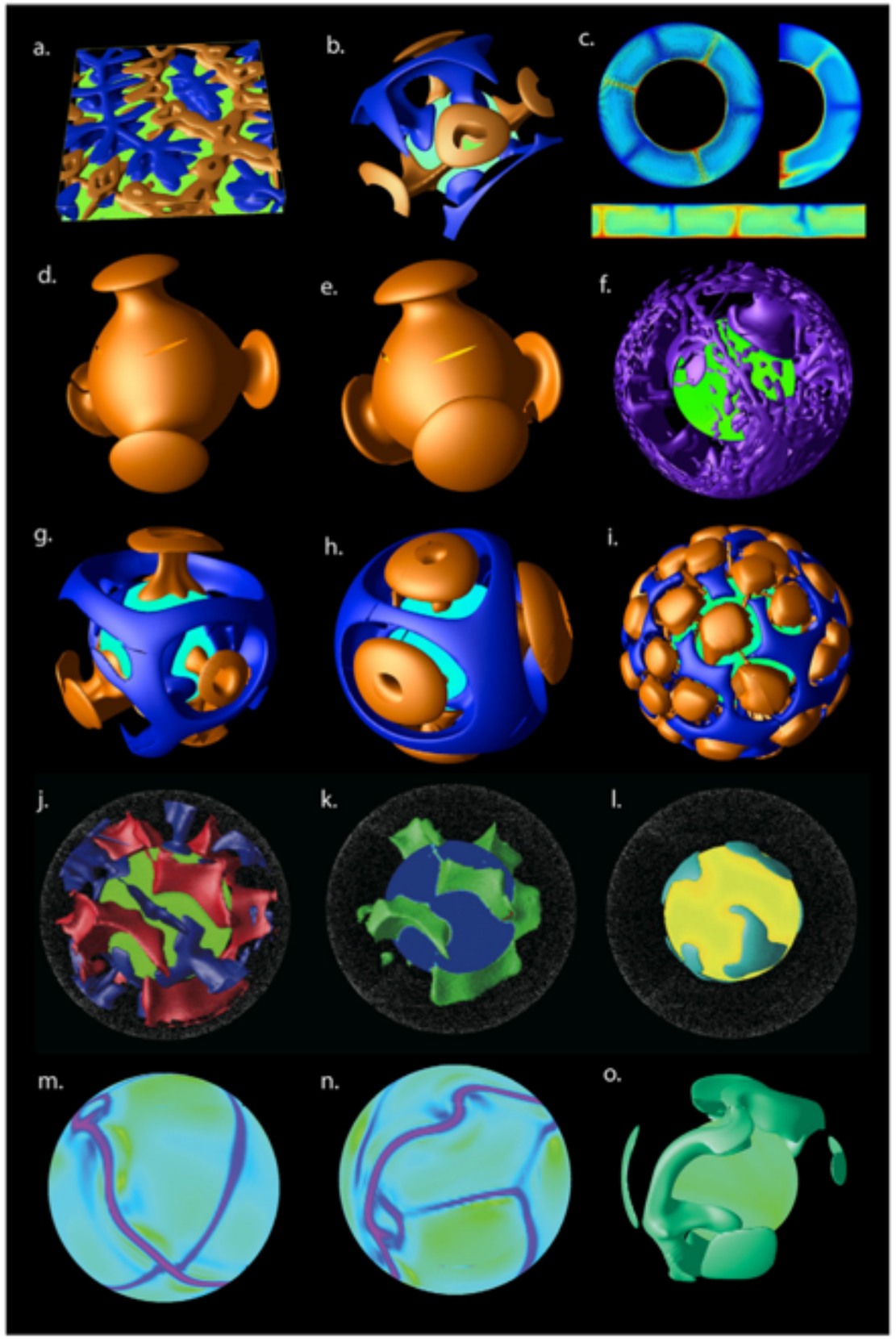

Fig. 1. Various results obtained with StagYY. The top row illustrates alternative geometries that can be modelled by changing one input switch, all for basal heated convection at $Ra = 10^5$: (a) cartesian, (b) spherical patch, and (c) 2D spherical annulus, spherical axisymmetric, or cartesian. (d) Isoviscous or (e) viscosity contrast 20 tetrahedral benchmark cases with $Ra = 7000$; isosurface of $T = 0.4$ is shown. (f) Compressible convection with an endothermic phase change at 670 km depth and parameters as in Tackley et al. (1993). (g–i) Basally heated convection at $Ra = 10^5$: isoviscous, viscosity contrast 10^3 or 10^6, respectively. (j) Residual temperature isosurfaces (k) composition isosurfaces and (l) post-perovskite for compressible thermo-chemical multi-phase convection discussed in (Nakagawa and Tackley, 2008), (m and n) viscosity in the outer layer and (o) temperature isosurface for internally heated convection with visco-plastic temperature-dependent viscosity, showing self-consistent generation of tectonic plates with parameters similar to Tackley (2000a,b) and van Heck and Tackley (in press).

(Tackley ,2008)

“The quest for self consistent tectonics”

YIELD STRENGTH

34 MPa

70 MPa

86 MPa

120 MPa

168 MPa

200 MPa

340 MPa

Continuous plates

Episodic plates

Rigid lid (no plates)

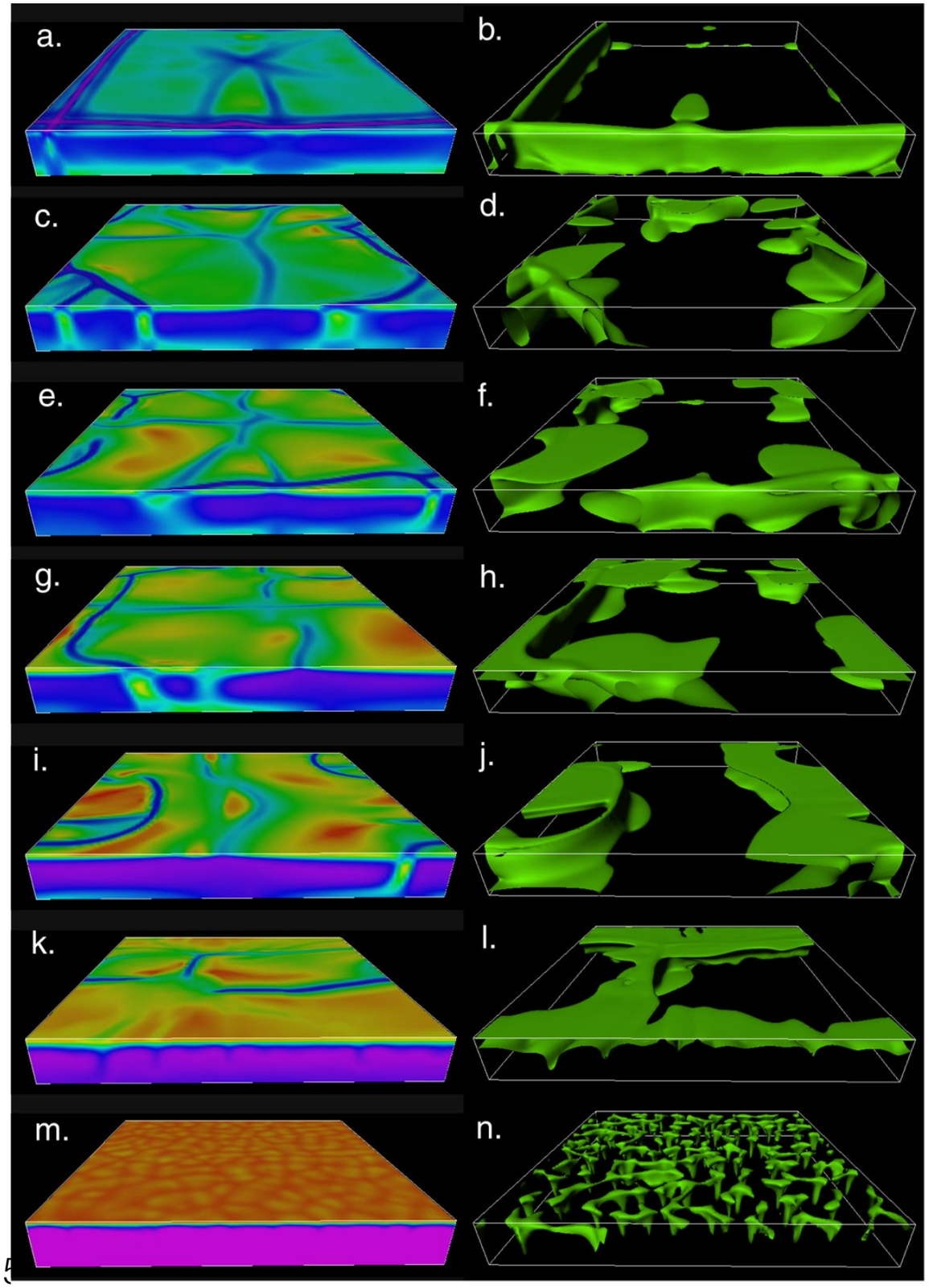

(Tackley ,2000)

“The quest for self consistent tectonics”

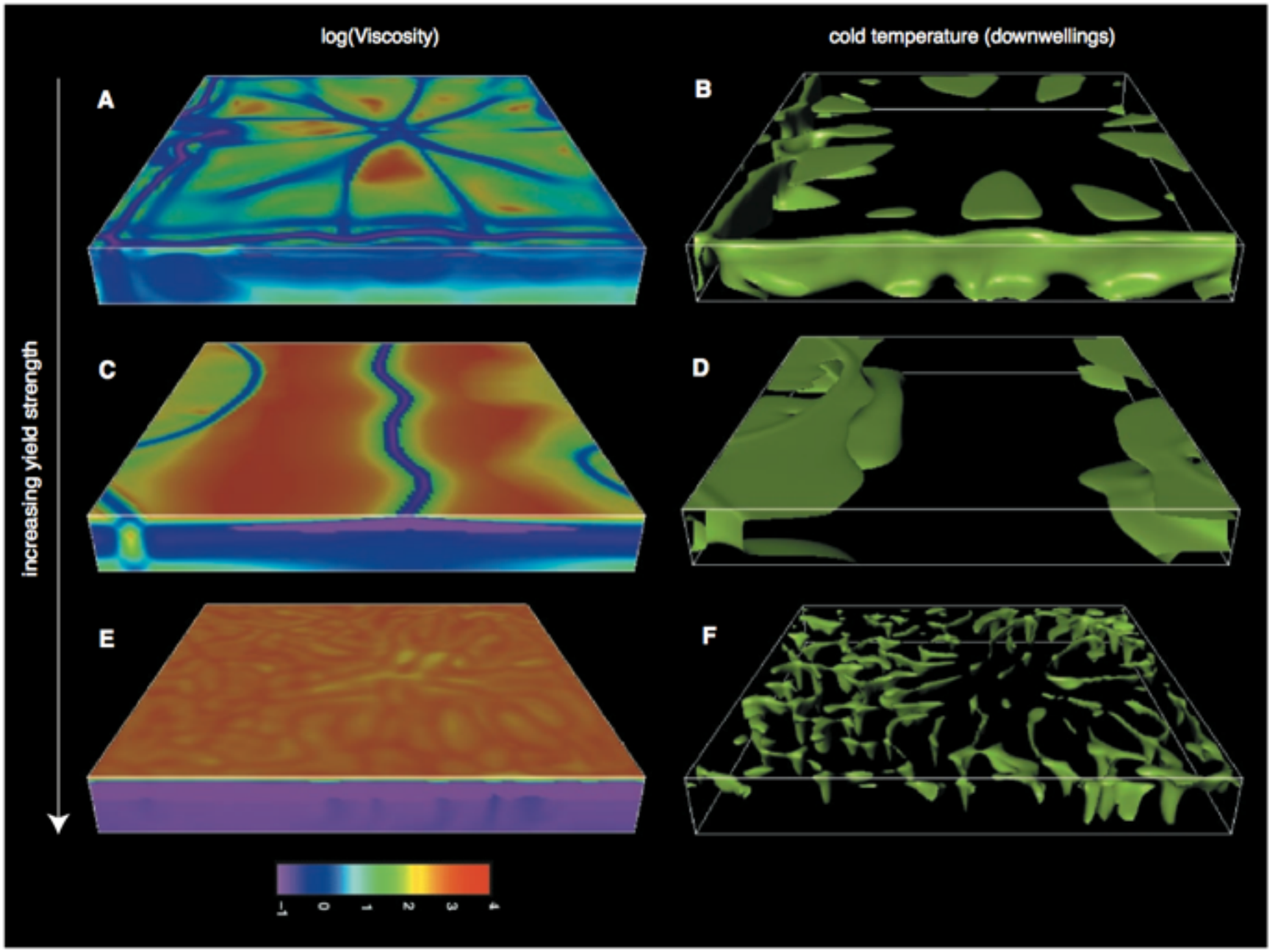

Fig. 1. Numerical simulations of mantle convection with self-consistently generated plate tectonics [from (*38*)]. The rheological model incorporates temperature-dependent viscosity varying by up to five orders of magnitude, a constant (with depth) yield stress, and a factor of 10 viscosity reduction when the temperature reaches the solidus. The left column shows the logarithm of viscosity relative to a reference mantle value; red corresponds to the strongest material and purple corresponds to the weakest material. The right column shows cold downwellings (where the temperature is 250 K colder than the horizontal average). System behavior depends critically on the yield strength: With low yield strength (**A** and **B**), plate-like surface motion is observed but plates are weak. With intermediate yield strength (**C** and **D**), plate-like behavior is observed with strong plates and weak boundaries. With high yield strength (**E** and **F**), rigid lid behavior is observed.

(Tackley ,2000)

“The quest for self consistent tectonics”

YIELD STRENGTH

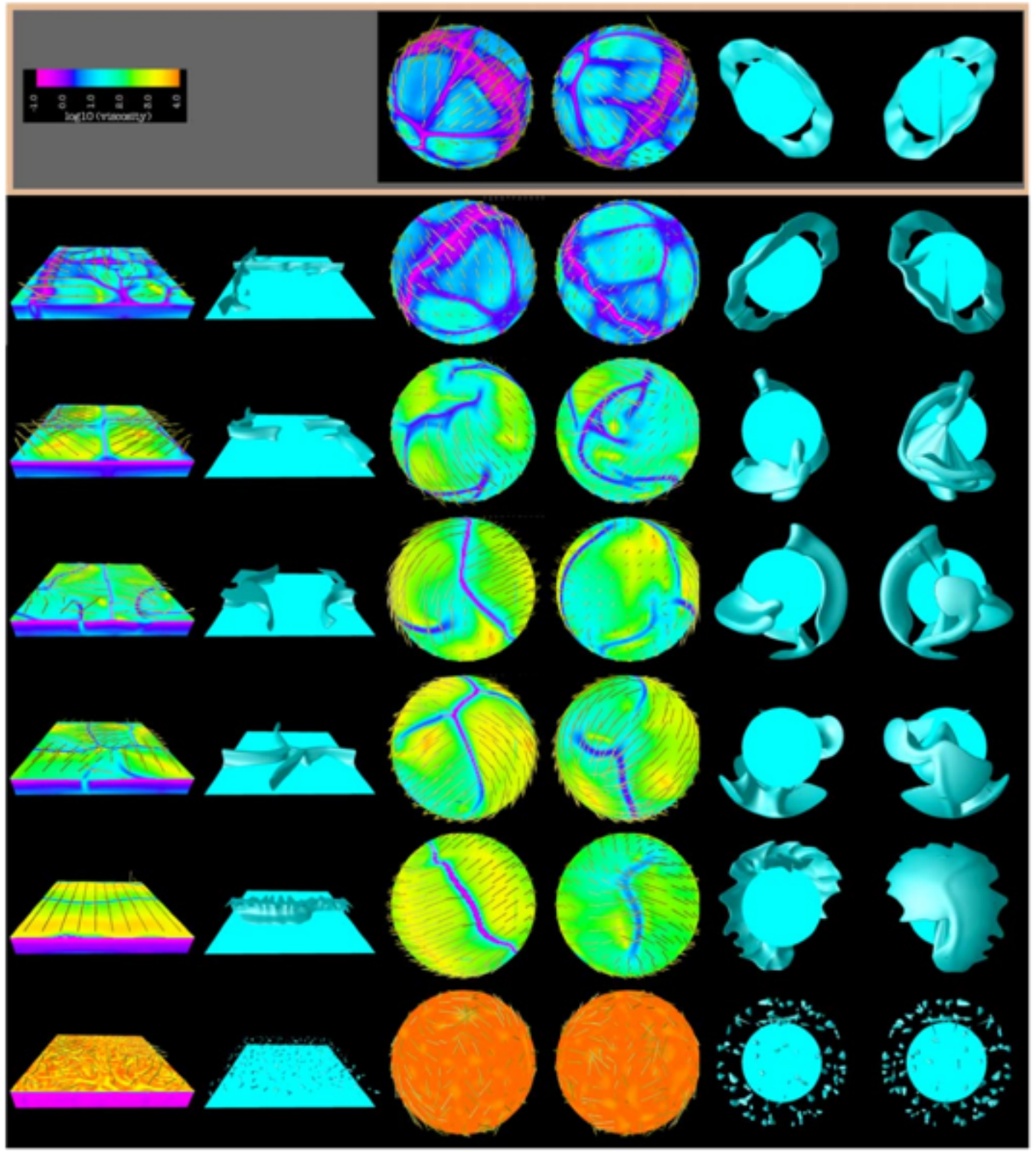

Figure 1. (left) The viscosity at the surface (z = 0.97), arrows indicate the velocity field. The narrow blue/purple zones represent weak zones, i.e., plate boundaries. Orange/red zones indicate rigid zones, i.e., plates. (right) The temperature where it is 17% lower than the horizontal average. For the spherical cases both sides of the sphere are printed next to each other. Yield stress increases from top to bottom as; $1.4 * 10^3$, $5.7 * 10^3$,$8.5 * 10^3$, $9.9 * 10^3$, $2.0 * 10^4$, $3.5 * 10^4$. The images show snapshots taken from each run. In the box at the top a snapshot similar to first calculation is shown but rotated arbitrarily.

(van Heck & Tackley ,2008)

Summary

- *Convective regimes are highly influenced by the form of the viscosity — and many other physical factors, e.g. internal heat sources*

- Care should be taken when discussing and comparing results of non-dimensional simulations
- Adding complexity (one at a time) into convection models can help the development of our understanding of fundamental processes relevant to the Earth (and other planets),…
- …however, non-dimensional analysis will only get you so far
- When “all” physics is included, disentangling the relevant importance of each, or determining the dominant contribution to a regime is difficult
- The “minimum” necessary physics to study any given convective process is not defined
- To date, there is no model which produces self-consistent plate tectonics, future research is required